Development and Validation of a Novel Single-Cell Attachment and Spreading Platform (Cell-STEPs) Utilizing Fused-Fiber Nanonets

Amritpal S. Gill

Thesis submitted to the faculty of the Virginia Polytechnic Institute and State University
in partial fulfillment of the requirements for the degree of

Master of Science
In
Mechanical Engineering

Amrinder S. Nain, Chair
Bahareh Behkam
Rakesh K. Kapania

May 6, 2015
Blacksburg, Virginia

Keywords: nanofiber, attachment, cell force, cell spreading, single-cell

Development and Validation of a Novel Single-Cell Attachment and Spreading Platform (Cell-STEPs) Utilizing Fused-Fiber Nanonets

Amritpal S. Gill

ABSTRACT

Initial attachment to the extracellular matrix (ECM) and consequent spreading is a necessary process in the cell cycle of which little is known. Cell spreading has been well-recognized in 2D systems, however, the native fibrous ECM presents cells with 3D biophysical cues. Thus, using suspended fibers as model systems, we present the development of a novel platform (Cell-STEPs) capable of capturing cell attachment dynamics and forces from the moment a cell in suspension contacts the fiber. Cell-STEPs comprises of a custom glass-bottom petri dish with a lid to deliver a constant supply of CO_2 to maintain pH. Fibrous scaffolds are attached in the dish to allow cellular investigations over extended periods of time. We find that cell-fiber attachment occurs in three progressive phases: initial attachment of cell to fiber (phase 0), rapid drop in circularity (phase 1), and increase in cell spread area (phase 2). Furthermore, using iterative inverse methods, forces involved in cell spreading through deflection of fibers were estimated. Our findings provide new insights in attachment biomechanics, including initial sensing and latching of cell to fiber with a negligible or protrusive force, followed by rapid loss in circularity through protrusion sensing at nearly constant spread area and minimal force generation, transitioning to a final phase of increased contractile forces until spread area and force saturation is observed. Also, anisotropic spreading of cells on single and two-fibers are closely related, while cells attached to several fibers take longer and spread isotropically. The Cell-STEPs platform allows, for the first time, detailed interrogations in the discrete and orchestrated adhesion steps involved in cell-fibrous matrix recognition and attachment along with simultaneous measurements of forces involved in cell attachment.

Acknowledgements

This thesis is the culmination of many choices, decisions, consequences and interactions. The next page is my humble attempt at recognizing everyone who has made it possible.

First off I would like to thank all three of my committee members who have provided insight and encouragement throughout this entire process - Dr. Nain for inspiring me nearly four years ago to expand my knowledge base beyond the typical mechanical engineering application and really question what we can do, Dr. Behkam for the wonderful assistance when working on the cell aspiration project and the biofab paper, and Dr. Kapania for the immense guidance in the force modeling.

I'd like to thank all of the other members of the STEP Lab – Kevin Sheets, Puja Sharma, Ji Wang, Colin Ng, Brian Koons, and my summer undergraduate assistant Paige Szymanski whom all provided an indescribable amount of help and direction as I entered and grew within the lab. I'd also like to thank members of the MicroN BASE Lab – AhRam Kim, Zhou Ye, and Chris Suh, whom I was able to work closely with on several projects. I wish you all the best as you step forward in your lives.

This is for those who were there for calls about nothing, for those who were there when no one else was, for those who were there for something as simple as a walk, for those who were there for the late-nighters, for those who were there for the 20-mile hikes, for those who brought back the taste of undergrad, and for those that have been there to get me where I need to be.

This is for my parents, who constantly encouraged me to achieve my best and no matter how tough the situation got, reminded me that they were always there for support.

This is for Robin, Blake, and Ike who are constant reminders of the simpler things, reminders of the important things.

All photos by author, 2015

Contents

List of Figures

List of Tables

List of Equations

List of Abbreviations

AFM	Atomic Force Microscopy
CO_2	Carbon Dioxide
DMEM	Dulbecco's Modified Eagle Medium
ECM	Extracellular Matrix
FBS	Fetal Bovine Serum
FN	Fibronectin
fTFM	Fibrous Traction Force Microscopy
IO	Inside-out
MEF	Mouse Embryonic Fibroblast
OI	Outside-in
P0	Phase 0
P1	Phase 1
P2	Phase 2
PEG-DA	Polyethylene glycol Diacrylate
PS	Polystyrene
PVDF	Polyvinylidene Fluoride
SCFS	Single-Cell Force Spectroscopy
SEM	Scanning Electron Microscope
SFK	Src Family Kinases
STEP	Spinneret-based Tunable Engineered Parameters
STEPs	Stochastic, Transient Extension Periods
TFM	Traction Force Microscopy
UDL	Uniform Distributed Loading

Chapter 1: Introduction

1.1 The Importance of Cell Attachment and Spreading

Initial cell attachment to its extracellular matrix (ECM) and consequent spreading are fundamental processes in the cell life cycle, however, little is understood on the cellular dynamics at play during these events. It has been documented that cells require substrate attachment in order to survive [1]. Attachment and spreading have been described to occur through one of two different methods: isotropically and anisotropically [2]. Anisotopic spreading has been described to take place through stochastic, transient extension periods (STEPs) which was not quantified in detail due to limitations in computer analysis [2]. Isotropic spreading has been covered in more detail and is thought to occur over three distinct phases which were first described by Döbereiner et al [3]. Since the initial recognition, many others have also shown this pattern of three individual phases of spreading occurring during early cell attachment to its environment [1,4–8]. These phases have been given different numerical numbers by the different groups, but here will be described as phase 0 (P0), phase 1 (P1), and phase 2 (P2).

1.2 The Three Phases of Spreading

Phase 0

Phase 0 begins with initial physical contact between the cell and substrate where the cell produces periodic, rapid membrane blebbing within seconds of contact [1,5,7]. Although blebbing is often associated with a cancerous phenotype or apoptosis, it also plays a very important role in early spreading [9]. It is well-known and accepted that the first step in adhesion is integrin binding to ECM proteins, which is one of the main events that occurs during P0 and is shown in Figure 1.

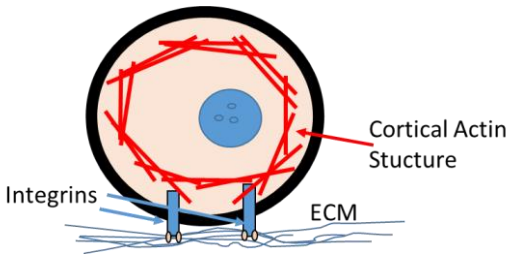

Figure 1. Diagram of phase 0 of spreading where cell-ECM contact is made. Initial bonding is stated to occur through Integrin-ligand bonding.

Effect of the ECM protein, such as fibronectin (FN), on attachment has been a key aspect that many of these groups have looked into. Most often, it is shown that increasing the concentration of ligand on the substrate leads to a larger percentage of attached cells and quicker initial attachment, while the following spreading dynamics are not altered [2,7,10]. The Sheetz group quantified attachment based on varying FN concentration, showing an eightfold increase in the percentage of attached cells when FN concentration was increased four times [2]. In this same study they showed with either increased or decreased ligand concentration, only a change in the initiation of spreading was effected, where lower concentrations led to increased delay in the onset of spreading from the time when the cell first contacted the substrate [2]. Another study, however, has shown that a relationship between the ligand concentration and spreading rate, where higher densities promoted isotropic spreading and lower densities led to anisotropic spreading [11]. One possible reason for this difference, mentioned in this work, was because different cell lines were used and this cell-line heterogeneity may lead to changing attachment dynamics [11].

Phase 1

The changeover from P0 to P1 occurs rapidly, with very little overlap in the defining actions of blebbing to continuous protrusion [2]. The main cellular action defining P1 is a rapid spreading of the cell body through continuous protrusion [1,4–6]. This is joined by increases in actin polymerization and retrograde actin flow as shown in Figure 2[1].

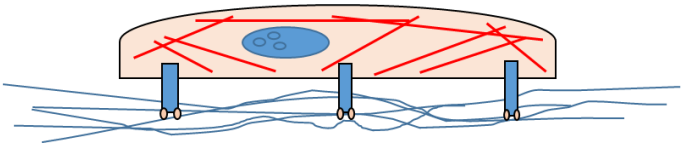

Figure 2. Diagram of phase 1 of spreading which is highlighted by rapid area expansion.

While the protrusive forces do increase in this phase, they are still relatively small [1,5]. One reason for this is that strong focal adhesions are not formed in this phase of attachment, where lamellipodia extend from the cell front to drive spreading [12]. While the lamellipodia protrusions extend forwards, there is a corresponding retrograde flow of actin within the cell which aids in rigidity sensing and regulating spreading speed [1,12,13]. The speed of retrograde actin flow is inversely proportional to the spreading speed with the sum of the two, corresponding to the rate of actin polymerization at the tip, remaining constant during spreading [2,12]. Looking at the distribution of paxillin, a focal adhesion protein, during this phase shows small dots spread randomly over the entire contact area of the cell explaining that strong clustering of focal adhesions not existing at this point [4]

Phase 2

The last phase of cell spreading, P2, is characterized by a continued increase in area, albeit at a slower rate, up to a saturated spread area [1,4,7,8]. The shift from P1 to P2 happens quickly, on the order of tens of seconds, leading to the assumption that the cell does not actively control motor activity to perform this switch [6]. Other key features of P2 include a maturation of focal adhesions, and the formation of actomyosin stress fibers which can be seen in Figure 3[1].

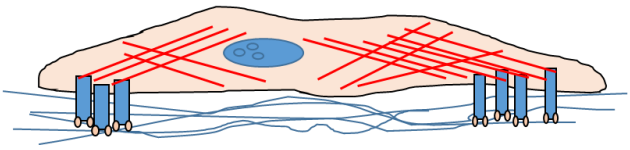

Figure 3. Diagram of phase 2 of spreading where focal adhesions mature and clear stress fibers are seen.

The retrograde actin movement within the cell that flowed slowly in P2 is now much quicker, and following the inverse relationship, spreading slows [12]. At this same time focal adhesions begin to cluster, as evidenced by a building intensity of paxillin fluorescence on the cell edge [4]. The final key characteristic of P2 is a high application of contractile forces by the cell [1,5]. This leads to an increase in cellular tension which reinforces focal adhesion sites through recruitment of additional attachment proteins [1,14].

1.3 Contractile Forces during Adhesion and Spreading

It has been shown that cell contraction, mediated by myosin, is a necessary function for cell spreading [15]. As described, this contractility does not come into play until P2 of attachment, where large traction forces are applied to the underlying substrate. It has been noted that these cell adhesion forces are dependent on ligand density, adhesion size, cell spread area, and environmental stiffness [4,16,17] Also, while much of the spreading dynamics follow lamellipodia expansion, it has been shown that focal adhesions develop at the edge of lamella, where the actin structure bear most of the load during spreading [4,18]. In cell adhesion force studies, it is commonly believed that development of focal adhesions and contractile force application by the cell are interdependent. Indeed, during attachment, groups have shown that tension at the actin-rich tip of the cell, is transferred to the lamella where forces encourage focal adhesion growth [4]. The first study on the cell force evolution during attachment was completed by Dubin-Thaler et al, utilizing deflecting micropillars [5]. Although imaging made measurements difficult in P0, they were able to demonstrate a force increase going to P1, with an even larger increase up to P2 before settling at a steady state [5]. However, there has also been recent evidence that considerable forces from the cell can be applied to its surroundings before any stable adhesions are formed [11]. In work by Reinhart-King et al, traction force microscopy experiments (TFM) have provided evidence that

cells exert significant traction forces as early as the first 30 minutes of spreading, while changes in actin polymerization are not seen until 60 minutes after spreading [11]. Further exploration in the same experiments have shown that the time scale for focal adhesion formation changes with ligand density. With the lowest concentration tested, 0.001 mg/mL, there were very few focal adhesions seen up to 24 hours later, while significant forces were seen quickly after attachment [11].

1.4 Dynamics of Cell Spread Area

A fundamental aspect of cell attachment studies is the characterization of the spread area maturation which signals at least one step of the cell attaining steady state adhesion, with both the chemical and mechanical environment an area of research. Following full cell attachment from initial contact to steady state adhesion, many groups have noted the total spread area to increase sigmoidally with time [7,12,19]. In work completed by Reinhart-King et al, it was shown that increasing the concentration of the ligand would lead to increasing cell spread area [11]. The ligand concentration was varied from 0.001 mg/mL to 1 mg/mL, a 1000x increase [11]. This led to a 6x increase in average steady state spread area, ranging from 1000 um^2 to 6000 um^2 [11]. Looking at the mechanical microenvironment, Cavalcanti-Adam et al manufactured nanopatterned substrates with either 58 nm, or 108 nm spaced ligands [14]. In comparison with a saturated substrate, cells plated on the closer spaced 58 nm ligands displayed a similar spread area while those on the 108 nm spaced ligand substrates had approximately half of the steady state spread area [14]. In addition to the smaller spread area, spreading initiation of cells on the wider 108 nm spaced ligand substrates was delayed while both the 58 nm spacing and saturated substrates were able to reach maximal spreading within two hours [14]. Analysis of this data showed that the cells on the 108 nm spaced substrates experienced greater retraction events due to not being able to

form solid adhesions leading to a spreading rate of approximately half of the other two conditions [14]. For similar reasons of increased retractions, anisotropically spreading cells experience over 2.5x slower spreading than isotropically spreading cells [2].

1.5 Statement of Problem

Cell attachment and spreading are feedback-driven processes where the cell is responding to both the chemical and mechanical environment surrounding it. Cell-matrix adhesion has been shown to correlate to biological processes such as morphogenesis and wound healing, with abnormal adhesion associated with diseased states such as cancer metastasis [1,8]. Using flat and gel substrates, excellent groundwork has been laid to understand these phenomena, but there is still much that can be done. In particular, all of the previously mentioned methods utilized either TFM or micropillar arrays as adhesion assays. While these provide great force measurement platforms, they lack the fibrous environment of the native ECM. In addition, the study of varying mechanical microenvironments is limited even though this has been mentioned as a key component in spreading propagation [6,12]. Utilizing the previously described Spinneret-based Tunable Engineered Parameters (STEP) method of manufacturing aligned and suspended polymer fibers, we bring forward a fibrous system intended to provide an environment more similar to the native ECM that is capable of creating specific architectures for studying cell attachment dynamics [20,21]. Using suspended fibers to study cell attachment dynamics requires development of a new platform which overcomes critical challenges in cell delivery to scaffolds already isolated in the incubating microscope. Since attachment is shown to occur on the order of minutes, this poses critical requirements of fast delivery of cells to the scaffolds in a non-destructive fashion, while also ensuring capability to image at high spatiotemporal resolution (20-40X magnification at less than 1 minute imaging interval). Furthermore, the platform also needs to provide continuous

supply of CO_2 to the scaffolds, thus ensuring management of pH levels critical for cell survival. Upon successful validation of the proposed engineered platform, detailed studies are conducted to understand cell area, circularity, and forces during cell-ECM attachment from initial contact to steady state adhesion

Chapter 2: Platform Development and Validation

2.1 Glass Bottom Petri Dishes

Cell delivery for attachment studies as well as the approach angle of the OI probe system required the use of petri dishes instead of 6-well plates. This was troublesome, however, since a majority of the petri dishes were plastic which would not allow for imaging at higher magnifications. In order to attain high quality images during force experiments, custom glass-bottom petri dishes were manufactured. These dishes utilize 'number 0' glass coverslips with thickness ranging from 0.08-0.13mm**.** This following section will outline the steps needed to produce one of these dishes.

Step 0 – Materials Needed

Before beginning the manufacturing, first gather all required supplies. These include a 55mm petri dish, a razor blade, a 22x22mm square piece of number 0 glass, a Dremel® rotary tool with drum sander attachment, and Loctite® all-purpose G02 glue as seen in Figure 4.

Figure 4. Tools and supplies required to produce a glass-bottom petri dish.

Step 1 – Initial Hole

The first step to manufacturing involves beginning the hole in the bottom of the dish. Press in the corner of the razor blade into the bottom of the dish as shown in Figure 5A and rotate the blade to cut open the dish. Continue this motion until the hole is approximately 10mm in diameter as seen in Figure 5B**.**

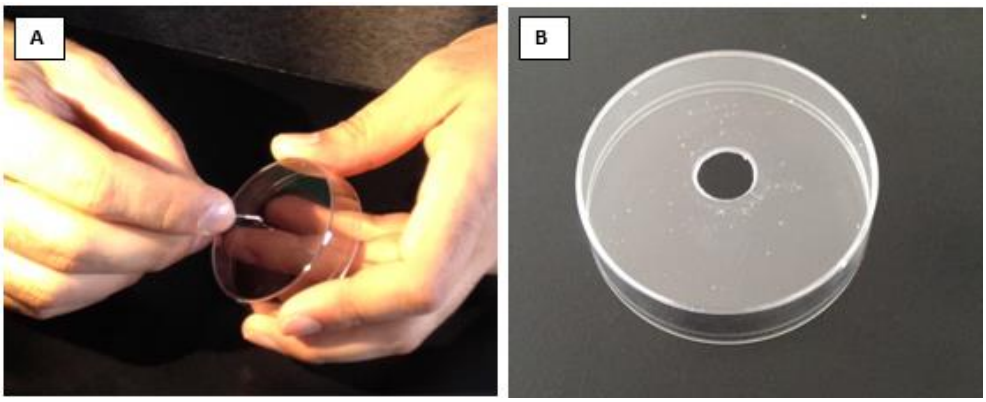

Figure 5. (A) Start the hole using the corner of the razor blade. (B) Enlarge hole until it is approximately 10mm in diameter.

Step 2 – Enlarge Hole

In this next step, the Dremel® sander is inserted into the hole and is used to enlarge to approximately 18-20mm in diameter. When using the rotary tool move in a counterclockwise motion, as this will provide more consistent cutting as seen in Figure 6A**.** The result at the end of this step is seen in Figure 6B.

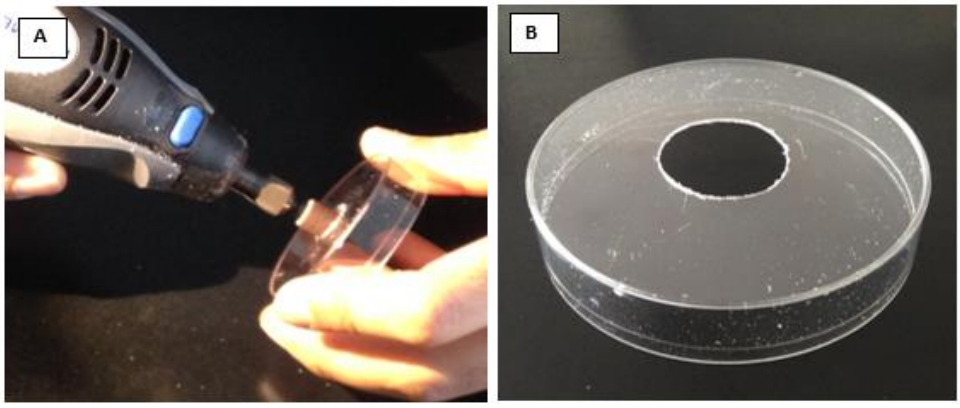

Figure 6. (A) Use Dremel® tool to enlarge hole. (B) Final hole diameter should be 18-20mm.

Step 3 – Deburr Edges of Hole

After enlarging the hole, there will be heavy burrs on the edges. This will cause problems with sealing leading to leaks so they must be removed. Use a razor blade or X-Acto knife as shown in Figure 7A to clean the burrs on both the inside and outside of the dish. When completed, the dish should look as shown in Figure 7B.

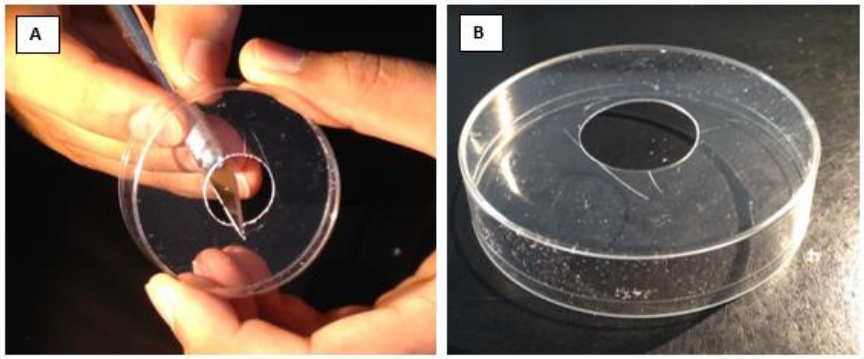

Figure 7. (A) Use an X-Acto to clean up the burrs from the Dremel. (B) Finished hole with smoothed edges.

Step 4 – Glue Glass Bottom in Place

After the hole has been cleaned, pour the glue around the outer edge as seen in Figure 8A, leaving approximately 1mm of space between the glue and the hole. This ensures excess glue isn't pushed inside limiting the usable area. Next, place the 22x22mm square piece of glass centered over the hole. As shown in Figure 8B, apply gentle finger pressure to the center of the glass in order to evenly spread the glue and set the glass.

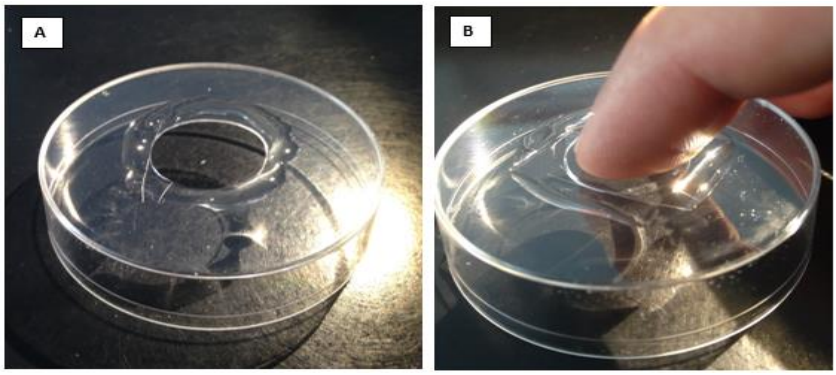

Figure 8. (A) Glue applied around the hole. (B) Place glass and apply gentle pressure from finger.

Step 5 – The Final Product

Within 30 minutes the glue will be set, but allow at least 24 hours for full-cure before using dish. The final product can be seen in Figure 9 below.

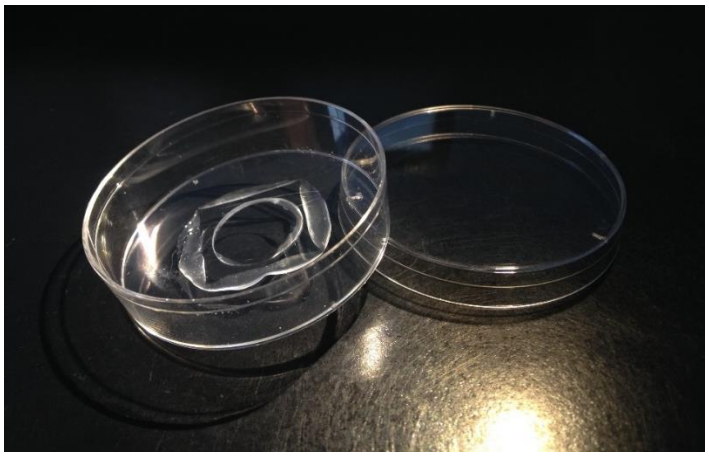

Figure 9. The final manufactured petri dish with glass bottom in place.

2.2 CO_2 Lid

As mentioned previously, probe work on STEP fibers requires an open-top dish, but this has resulted in experiments that must be run very quickly in order to maintain a viable pH for cells. Other solutions used in the past included using different media or supplementing the media with HEPES as a buffer in order to maintain pH. This, however, introduces another variable into the experiments that may have biological repercussions in cell behavior. In order to help remediate this situation, carbon dioxide (C02) lids were manufactured for both the 25mm and 55mm petri dishes. These lids were created using similar methods to the glass-bottom petri dishes so the process will not be discussed in detail. Figure 10 shows the lid for the 55mm petri dish, with (A) showing the outside-in variation and (B) showing the inside-out setup. The large hole in the top allows room for the micropipette to move around freely anywhere on the scaffold and is created by starting a hole using a razor blade and enlarging with the Dremel® tool. The hole for the CO_2 line is created using just the razor blade. The CO_2 tubing is secured to the lid using biocompatible

cyanoacrylate (superglue). Additionally, a counterweight must be placed opposite the tubing in order to keep the lid balanced. Standard tack putty was used to maintain this balance while in use.

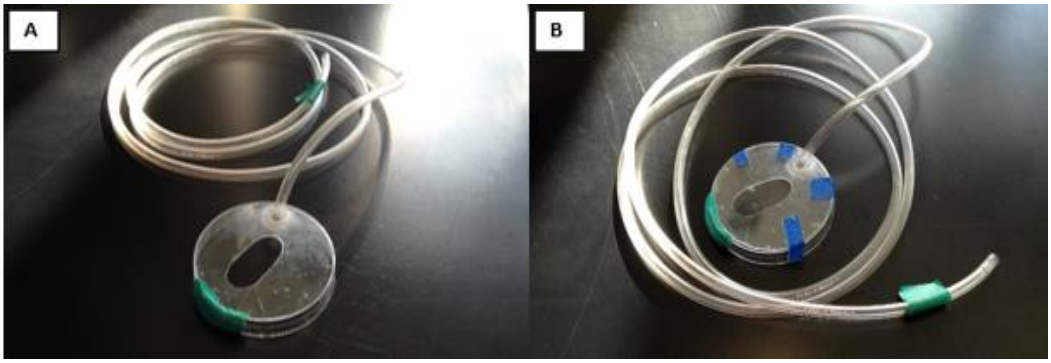

Figure 10. (A) CO_2 lid for use in outside-in probe experiments. (B) The same lid modified to use for inside-out experiments.

The only change required to go from outside-in to inside-out is the addition of a cover piece which is seen in Figure 11. This cover piece was created by using a 55mm petri dish lid and removing the side overhangs using a razor blade. Next, a small square portion was cut in order to have it fit around the CO_2 tubing. Finally, a small hole was created using a razor blade so that 1.09mm diameter ethylene oxide micro medical tubing would fit snugly to allow for both cell and drug delivery to a scaffold mounted inside of the petri dish. The addition of this lid allows for imaging over many hours without losing media to evaporation which may occur with the large hole used in the outside-in setup.

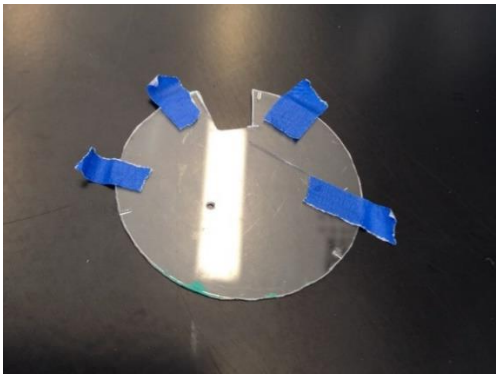

Figure 11. Cover placed on CO_2 lid when probe work is not needed. The small hole for the tubing and cutout for the CO_2 line can be seen.

When in use, the lid provides CO_2 enriched air as required, while simultaneously not interfering with imaging. Figure 12 below shows the lid in use for outside-in experiments (A), as well as inside-out experiments (B). In both, the drug delivery tube is shown placed into the dish and for outside-in the clearance available to the probe can be seen.

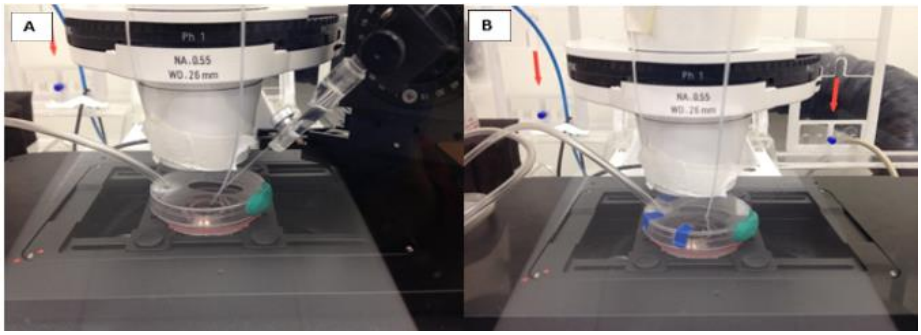

Figure 12. (A) CO_2 lid in use for an outside-in experiment with both probe and drug delivery tube in place. (B) CO_2 lid in use for an inside-out experiment with cover piece and drug delivery tube.

In order to confirm a functioning product, testing was conducted to verify pH over an extended period of time. A piece of litmus paper was dipped into cell culture with passage 40-43 DBTRG-05MG cells in RPMI-1640 media every five minutes for four hours. Figure 13 shows the four trendlines corresponding to each test. Each experiment resulted in the pH settling and holding at 6.8. This is lower than the ideal case, but is expected when using RPMI-1640 media since it is supplemented with a small amount of HEPES.

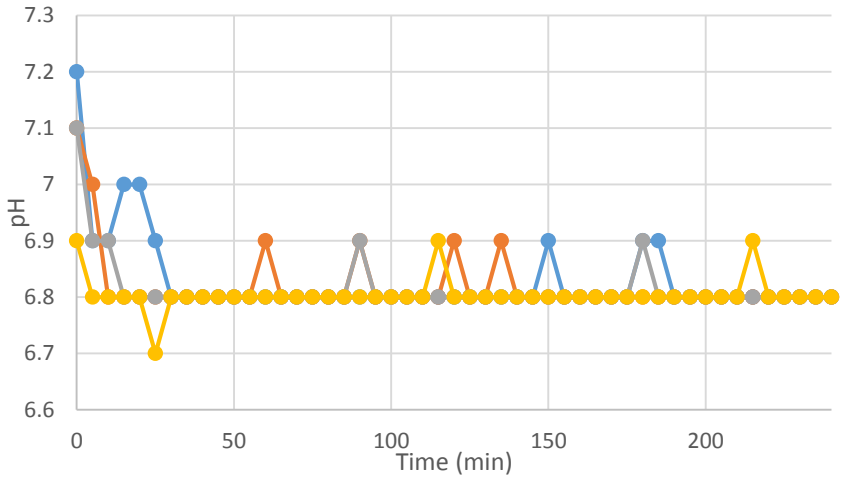

Figure 13. Stabilization of pH over four hours when using CO_2 lid on 55mm petri dish.

2.3 Fiber Fusing Using a Desiccator

One of the major advantages of the STEP fiber system is the ability for consistent fiber collection. The current fusing system in place is based around very quick, on the order of ~1 second, exposure of a scaffold to solvent vapor. This, however, can potentially cause variances in a sample that that was spun in a consistent fashion since a fraction of a second difference in time will change the amount of fiber that has dissolved. This problem was addressed by looking into a system where the time scale was longer allowing for more controlled fusing. The method chosen was to use a 170mm Plate I.D. Wheaton Dry Seal™ Desiccator seen in Figure 14 which would move fusion time to the order of minutes. Other required supplies also shown in Figure 14 include SEM pin mounts with double-sided copper tape to mount scaffolds, needle-nose pliers to load and unload the aluminum tray, glass micropipette to add and remove solvent from the pyrex dish at the bottom of the desiccator, and Tetrahydrofuran (THF) as the solvent for fusing. The aluminum tray loaded with SEM pin mounts can be more clearly seen in Figure 15. The pin mounts are placed at equidistant radial positions in order to promote consistency between fused scaffolds. Testing was done on a standard force scaffold with ~800nm diameter boundary fibers and ~350nm diameter deflecting fibers manufactured using 10% polystyrene (PS) in xylene (w/w) and 6% PS in xylene (w/w), respectively.

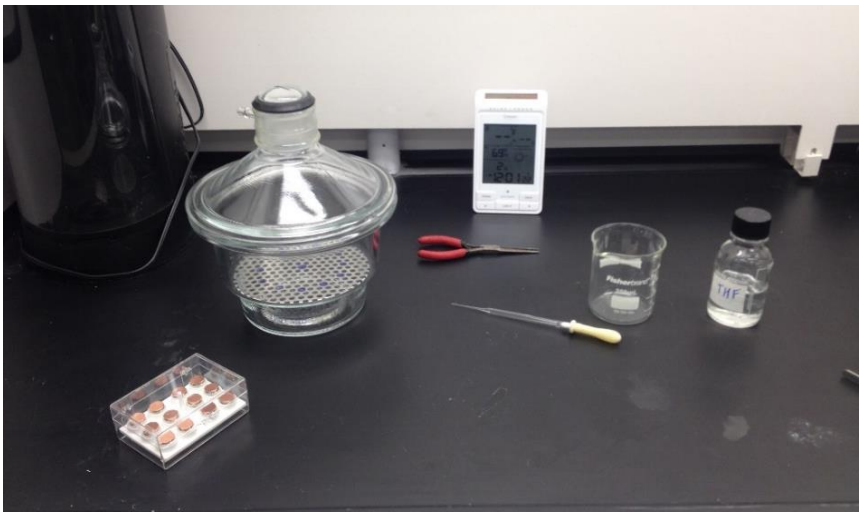

Figure 14. Supplies needed for fusing scaffolds using desiccator.

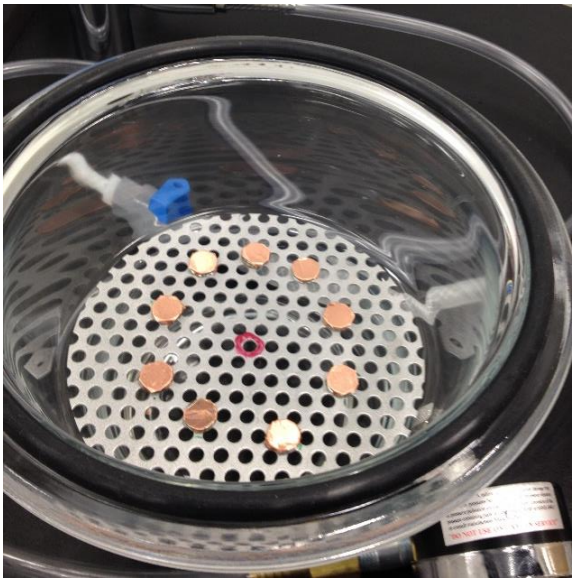

Figure 15. SEM pin mounts loaded into the desiccator on the aluminum tray.

Determining optimal fusion times was a trial-and-error process with variables of both vacuum pressure and time. Table 1 outlines some of the trials run along with the resulting fiber structures. At first it was determined that using vacuum pressure would cause very long fusion times, so no vacuum was run leaving time the sole independent variable. Through this, 8 minutes of THF vapor exposure was determined to be the optimal fusion time for 10% PS to 6% PS which was confirmed by performing probe pulls on the fibers as shown in Figure 16.

Table 1: Example trials with results when testing for fusion of 10% PS to 6% PS

Vacuum Pressure (in Hg)	Time (minutes)	Result
-10	45	Heavy fiber damage
-10	30	Bottom layer fused, top layer is not
0	30	Lots of fiber damage
0	3	No fusion
0	15	Hole in bottom layer, top looks good
0	10	Minor fiber damage
0	8	Fused top and bottom layer

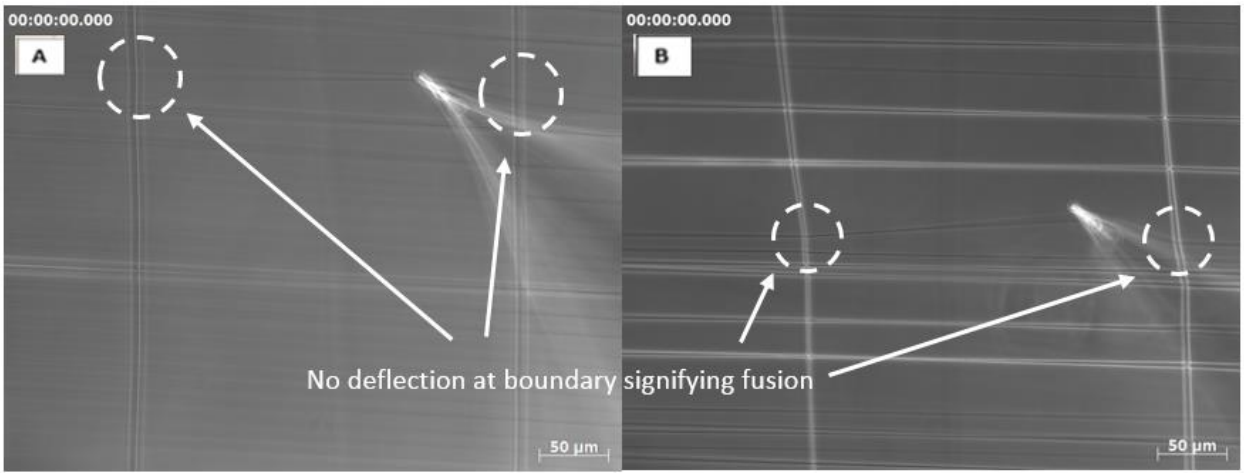

Figure 16. (A) Glass micropipette pulling on a fiber from the top layer of fibers showing fused boundary conditions. (B) Glass micropipette pulling on a fiber from the bottom layer of the same fused scaffold.

To further the practicality of the desiccator fusion system, a similar trial-and-error approach was used to characterize fusion times for other commonly spun scaffolds. An outline of the required time to fuse when no vacuum pressure is used can be seen in Table 2.

Table 2: Fusing time for various polystyrene solution concentrations

Fiber Solutions	Time (minutes)
6% PS to 10% PS (350nm on 800nm)	8
4% PS to 10% PS (200nm on 800nm)	4
10% PS to 10% PS (800nm on 800nm)	10
6% PS to 6% PS (350nm on 350nm)	6

2.4 Effect of Rapamycin on Force Output from Mouse Embryonic Fibroblasts

2.4.1 State-of-the-art Force Measurement Systems

Cell traction force generation is a key biological process for everything occurring inside of the body including both development and disease. These traction forces are exerted at cell-substrate attachment points called focal adhesions and are used for various cellular processes such as migration, extracellular matrix (ECM) remodeling, and physically linking cells to other cells and tissue [22,23]. Different cell types (bone, muscle, fat, etc.) have specific functions and their forces will vary. The goal behind traction force measurement is to better characterize the mechanical properties of cells. Relationships between cell behavior and the mechanical properties of the surrounding environment can be made by measuring the forces through *in vitro* experiments. By characterizing forces *in vitro*, we can get extrapolate to how cells migrate/differentiate in the body and apply that towards studying both development and disease. Some of the common current force measurement assays are described as follows.

AFM-Based Single-Cell Force Spectroscopy

One well-accepted cell force measurement technique is single-cell force spectroscopy (SCFS). This method uses functionalized atomic force microscopy (AFM) cantilevers to study

adhesion dynamics of cells down to a single molecule [24–26]. Cell adhesion can be investigated through different loading of the SCFS system. For one process, cells that are adhered to a surface are contacted by the functionalized AFM tip for a set period of time, allowing bonds to form between the cell and tip. After this time, the tip is retracted from the cell and the deflection of the cantilever provides an adhesion force [25]. The other way SCFS is often used is for cell-cell adhesion studies by having a cell adhered to the cantilever tip and then contacting another cell. Similar to before, the cells remain in contact for a certain period of time before retracting the AFM tip [25]. This method allows for investigation of both cell-environment and cell-cell bond dynamics. By varying contact time, the temporal adhesive properties can also be studied[26]. AFM-based SCFS is a very powerful method to study cell adhesion. It can provide very detailed information for a single cell, with a high level of precision giving adhesive forces down to the range of piconetwtons and single molecules. However, to acquire statistically significant data, many experiments must be run which can be very time consuming. Also, one must have access to specialized AFM equipment and be trained in using the tools.

Nanotweezers

A new twist on AFM-based SCFS uses the same principles of a deflecting cantilever beam but applies it twice in the form of a tweezer [27]. This method utilizes two independent nanoprobes to "pick" cells. Using the nanopositioning stages, the cell is pulled upwards until it releases from the substrate. The deflection of the cantilever beam probes here will give the attachment force of the cell. This new technique sees many improvements and advantages over the AFM system it is based including easier loading and removal of the cells on the cantilevers. The nanotweezers do not need complicated and labor-intensive cleaning or replacing of the cantilever tip between different cell runs. This allows higher efficiency with the ability to run many more experimental

trials daily. There are a few limitations, however, such as a lower resolution compared with AFM if using the same probe since there are now two tips per cell. It is also difficult to use on cells that have spread since the nanotweezers will peel the edge of the cell.

Nanopillars

Another widely used and accepted method to measure cell forces is nanopillar arrays. Polymeric nanopillars in this study are made using nanosphere lithography which is outlined in Kuo et.al. [28]. This technique allows for the creation of nanopillars with varying diameter and spacing. These pillars can then be modelled as cantilevers with stiffness characterized through AFM measurement. The deflection of each of these pillars, measured as the change in position of the center of each pillar, will then correlate with the traction force that the cell is applying. With cells seeded on top of the nanopillar scaffolds, many of the pillars will be deflected at once which will give the changing traction force overtime as the cell moves. Nanopillar arrays offer great benefits in that forces applied across many different focal adhesion points can be visualized and calculated. Using nanosphere lithography to manufacture the pillars allows for control over the size and spacing between pillars which in turn can give different resolutions in force measuring. These are also easy and quick to produce aiding in the use for experimentation. One disadvantage, however, arises when functionalizing the pillars. With it being very difficult to just functionalize the tip of the pillar, it is possible that the cells have focal adhesion points at various heights on the pillars causing error in the calculated force values.

Traction Force Microscopy

The method of using a deformable elastic substrate to measure single cell forces has been around since the 1980s [29]. By using a thin layer of material, deformations could be visualized as a cell moved across the substrate. Through the years this method has been improved upon using

newer materials such as polyacrylamide gels [30]. These gels, while being based on the same principle of a deflecting substrate, can be fine-tuned at various different stiffness's. Different stiffness values can be utilized to study the effect of environmental stiffness on cell traction force generation. For example, 3T3 fibroblast cells respond to the stiffness by producing fewer large stress fibers, polarizing their motion, and becoming more migratory on soft substrates [30]. Using this method can allow for a great visual of the cell morphology in response to the stiffness, however, limitations still exist for the system. The traction force measurements are very calculation intensive and the substrates are 2D gel environments, while the native ECM is a 3D fibrous structure.

2.4.2 Force Measurement with STEP Fibers

One recurring disadvantage shared by the previously mentioned methods of cell traction force measurement lies in the substrates used. Cells in their natural environment inside of the body are attached to a fibrous ECM network which is made up of protein fibrils that are 30-70nm in diameter and can bundle into fibers of 200nm to 1um in diameter. This ECM provides both a mechanical and chemical environment for cells to interact, allowing force generation for activities such as cell migration and ECM remodeling. The STEP method, a nonelectrospinning method of micro/nanofiber collection, has shown to be able to produce polymeric fibers of the same range with a high degree of control over the desired diameter as well as alignment and spacing of the fibers [20,21]. Additionally, detailed hierarchical structures can be manufactured to control pore size of the scaffolds and attempt to capture native *in vivo* environments [31]. Previous experiments utilizing the precise control on manufacturing of STEP fibers have begun to study the role of the mechanical environment on cell behavior through investigations of structural stiffness, curvature, and geometry on single-cell migration [32,33]. Further work with the STEP fibers has utilized the

system as a force-based drug testing platform [34]. This system can be thought of as a fibrous traction force microscopy (fTFM) method. Single-cell forces can be characterized as either outside-in (OI) which is the cellular response to an outside perturbation or inside-out (IO) which is the internally developed cellular force relating to adhesion and migration on its environment. The external perturbation for OI force experiments is applied by lifting the top of the two fibers a cell is suspended between using a glass micropipette controlled with a motorized micromanipulator. The deflection of the bottom fiber then corresponds with the cell force. This fiber deflection is also what is noted when studying IO forces, but in this case the cell is modulating its force in response to the environment to create this deflection. These concepts were investigated in further detail in a study showing these STEP fibers used as drug testing platforms [34]. Both IO and OI forces of the DBTRG-05MG cell line were analyzed in response to the addition of a varying concentration of cytochalasin D, a cytoskeleton altering drug which disrupts the organization of actin. The precision offered from the platform was able to show decreasing force response for both the IO and OI testing as well as a reduction in cell spread area.

The unique capability available through the STEP technique is manufacturing scaffolds with fibers specific to the desired application. The force measurement scaffolds, as seen in Figure 17 are manufactured using large diameter fibers (~800nm) vertically with small diameter (~350nm) horizontally. These are created using 10% polystyrene in xylene (w/w) spun at 300,000 steps/sec with a translational rate of 1.5 mm/s and 6% polystyrene in xylene (w/w) spun at 400,000 steps/sec with a translational rate of 0.08 mm/s. Outer dimensions of the substrate were kept constant at 6x6 mm as varying this will effect spacing between fibers. The resulting nanonet of fibers is then fused in a solvent vapor creating fixed boundary conditions at all intersections.

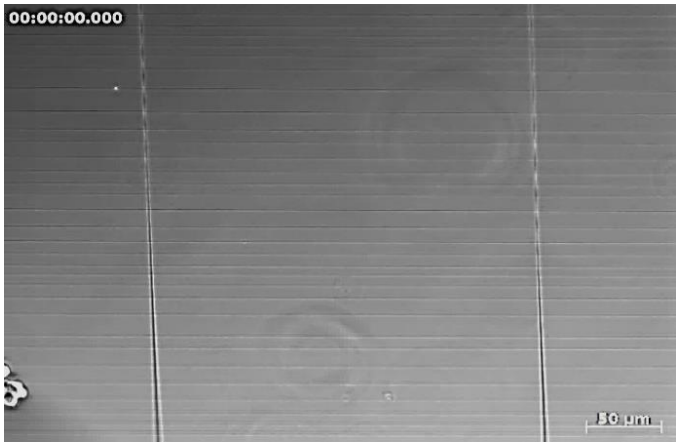

Figure 17. Sample of a force-testing scaffold with 800nm diameter boundary fibers and 350nm diameter deflecting fibers fused at all intersections.

Force analysis has been completed assuming uniform distributed loading (UDL) from the cell on the fibers. This was chosen based on fluorescent imaging that shows that focal adhesions exist across the entire section where the cell is in contact with the fibers. Shown in Figure 18 is a fluorescent-stained image where the green corresponds to paxillin – a focal adhesion protein. This green, although not always evenly distributed, occurs along the entire cell body and can be approximated by UDL. The fibers themselves are modeled as beams in tension with fixed-fixed boundary conditions as shown in Figure 19A. The deflections are small enough to maintain the fibers in the elastic deformation region. The derivation and closed-form solution for the UDL force can be seen in Appendix A. All cells studied are suspended on the deflecting fibers with no interaction with the base layer. This allows for analysis assuming only vertical force application on the fibers. Representative images of cell morphology in IO and OI force testing are shown in Figure 19B and Figure 19C, respectively.

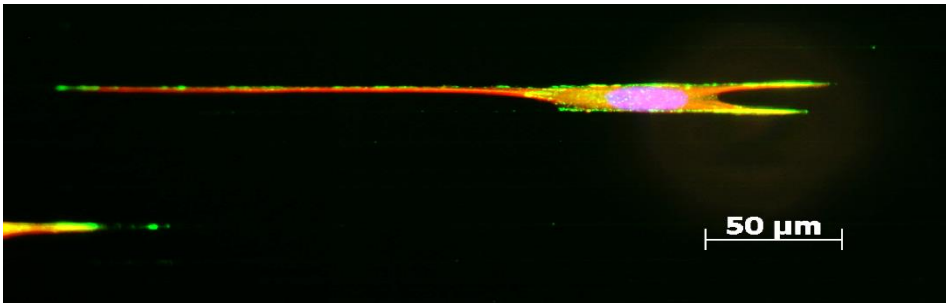

Figure 18. Fluorescent stain of MEF-Src showing actin (red) paxillin (green) and the nucleus (blue).

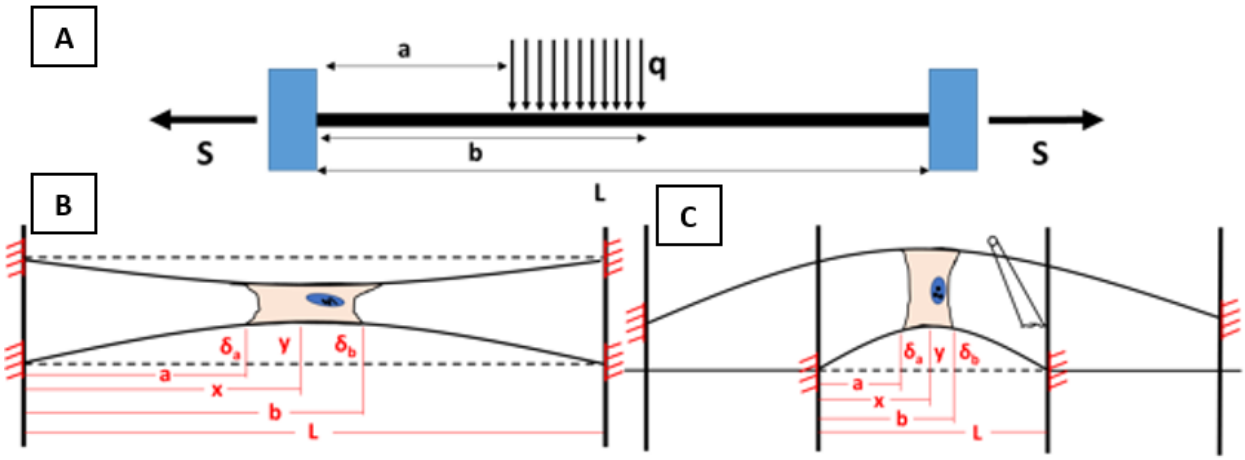

Figure 19. (A) Model of the fiber as a beam in tension. 'S' is the tensile force, 'a' is distance to the closest attachment point of the cell, 'b' is the other extreme point of attachment of the cell, 'L' is the length of the fiber, and 'q' is the load. (B) Schematic of IO force measurement. (C) Schematic of OI force analysis.

2.4.3 Results

After creating the tools necessary for OI force testing, experiments were run on mouse embryonic fibroblasts (MEF) which were engineered by the Hahn Lab at the University of North Carolina to selectively activate either the Src kinase (MEF-Src) or the Fyn kinase (MEF-Fyn) upon uptake of rapamycin. Both of these are members of the Src family of protein kinases (SFKs) which regulate cell signaling and processes through surface receptors [35]. Some of these processes include cell growth, differentiation, shape, migration, and survival [35]. The Fyn and Src kinases in particular have also been noted to have a role in cancer metastasis [36]. There has also been indication that SFKs are involved in cell adhesion dynamics since many Src-related elements such

as paxillin, talin, vinculin , and FAK [37]. The original protocol provided by the Hahn group called for using Dulbecco's Modified Eagle Medium (DMEM) supplemented with 10% Fetal Bovine Serum (FBS) for culture conditions and experimentation with DMEM supplemented with 2% FBS. The media needed to be switched several hours before experimentation according to this protocol so as not to induce the cells with the FBS concentration. However, during the beginning stages of testing, the cells did not respond well to this protocol. As seen in Figure 20, the cells showed a starved phenotype when sitting in 2% FBS medium for several hours. Through further experimentation a new protocol, which can be seen in Appendix B, was established. This protocol was next approved by the Hahn lab and was used for all further testing.

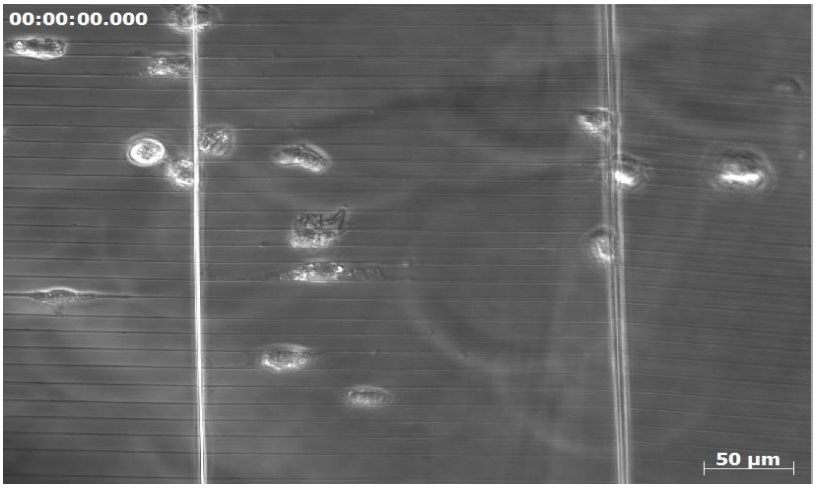

Figure 20. Starving MEFs when following protocol received from UNC.

Once the protocol was established and experiments were underway, other problems arose with the probe drifting several microns while experimenting. This was due to thermal fluctuations occurring inside of the microscope because of a dirty air filter. The issue this caused was that the probe would pull the top fiber to a different location after approximately 10 minutes. Pulling the top fiber to a different position will inherently bias the cell to output a different force. To address this issue, a method of standardizing the pull position of the probe was created using a transparency laid over the computer screen to mark the location of maximum pull. When setting up the

experiment, a dry-erase marker was used to mark the starting location of the probe, as well as the tip of the probe and fiber deflection at maximum deflection as seen in Figure 21. After every three pulls, since these were done every three minutes, the probe position was reset to the values on initial setup. When doing measurements post-experiment, this transparency method was again used to verify that the probe was being pulled to the same point throughout the experiment.

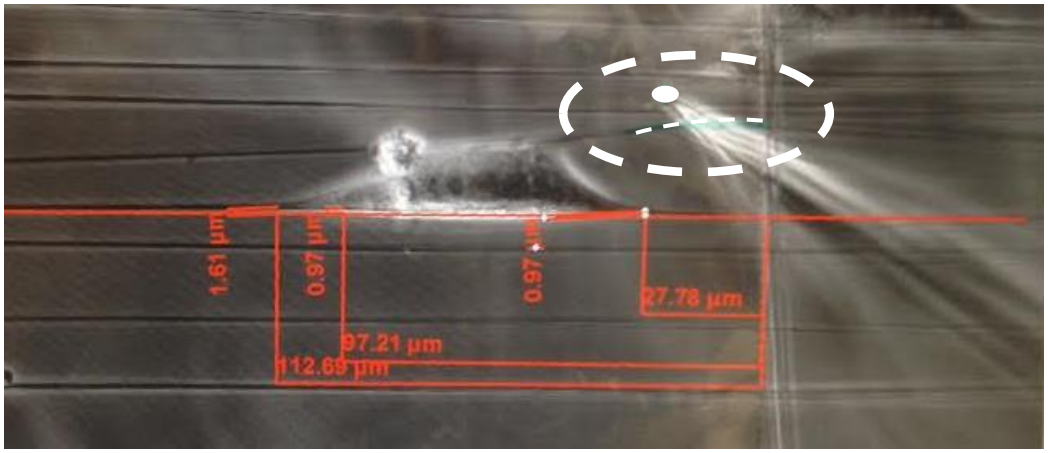

Figure 21. Standardization process of force probe pulls with locations of max pull marked by green dry-erase marker on the transparency.

Force analysis on the MEFs was done assuming UDL and calculating using inverse mathematics though a Mathematica program provided by Brian Koons. Analysis was also done on a normalized scale, so the relationship and change in force was the most important examination. During experiments, the top fiber was deflected a set distance once every three minutes for an hour. During the first 30 minutes, the cells were tested in standard experimental conditions with an example visible in Figure 22A. At the 30 minute mark, rapamycin was added to the medium at a concentration of 500nM and pulls were continued at the same rate of one every three minutes. An example of the response 21 minutes after adding rapamycin can be seen in Figure 22B. Figure 22C displays the relatively steady force response from both the Src (n=7) and Fyn (n=4) cell lines up until the addition of rapamycin where a transient decreasing force response is seen. This decreasing force corresponded with increased stretching and elasticity of the cell. While initially

the cell was fairly rigid, with the addition of rapamycin the cell was seen to stretch more. It has been reported that upon activation of the Fyn and Src kinases, cells have shown increased spreading [36]. This corresponds with the findings from the OI force experiments because the cells were seen to stretch more when the top fiber was pulled after the addition of rapamycin to active the kinases.

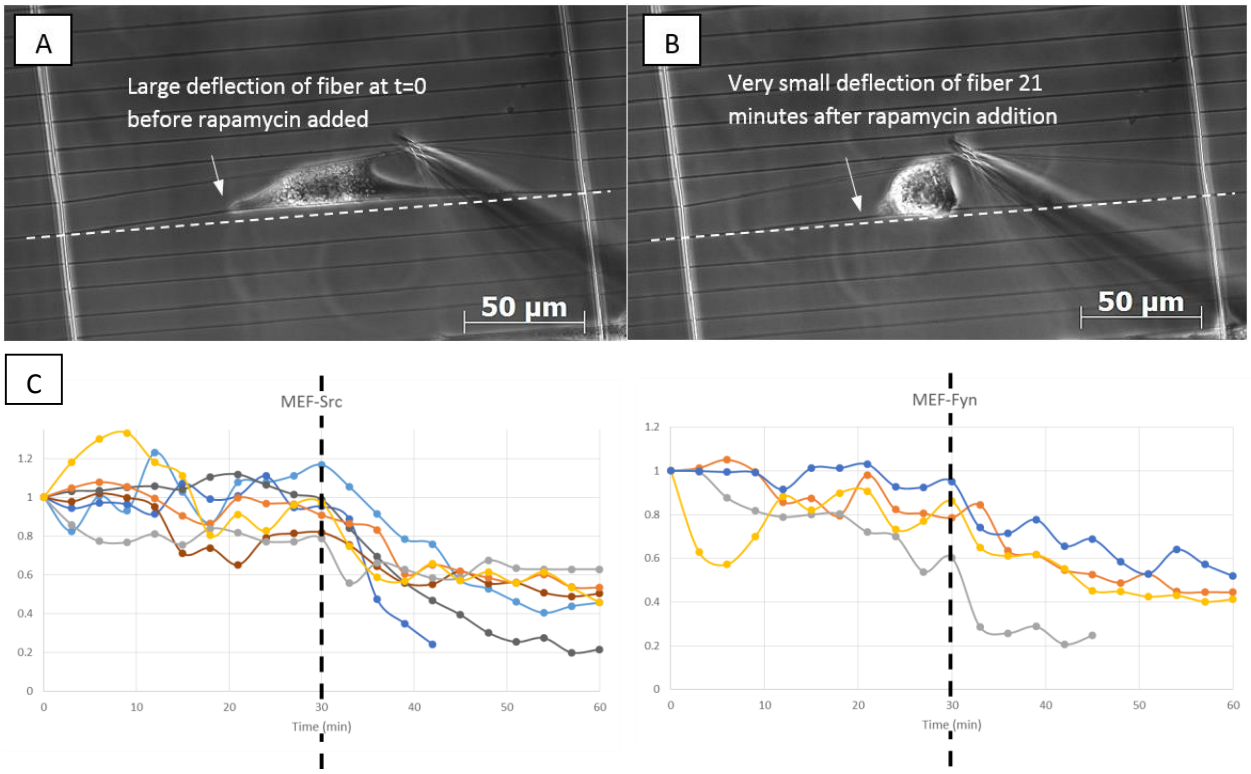

Figure 22. (A) OI probe pull with large fiber deflection by MEF-Fyn cell before adding rapamycin (B) OI probe pull 21 minutes after adding rapamycin. Cell assumes a rounder morphology and applies lower force to fiber. (C) Decreasing force response of MEF-Src and MEF-Fyn as rapamycin is administered after 30 minutes.

Chapter 3: Attachment Dynamics

3.1 Design of Scaffolds and System

Scaffolds were prepared by spinning PS fibers on 6mm x 6mm outer dimension plastic substrates. The inner dimension was designed to be smaller than usual at 2mm x 2mm so that imaging could be done at a high frame rate while maximizing the probability of capturing a cell in each frame. Wanting to study the effect of the mechanical microenvironment on attachment, manufacturing parameters were varied to create a collection of different substrates to study cell attachment dynamics.

3.1.1 Polymer Solution Preparation

One aspect of this varying microenvironment was the fiber diameter. All fibers were manufactured by dissolving polystyrene (Mw: 2,257,000 g/mol) in xylene by weight. Fiber diameters were chosen to be small (~200nm), standard (~350nm), and large (~800nm) which were created using 4%, 6%, and 10% PS, respectively. Boundary fibers were always created using the ~800nm fibers from the 10% solution.

3.1.2 Fiber Deposition

The other aspect of the microenvironment that was changed was the fiber spacing. This was done by changing the translational rate of the stage while spinning and provided for close (~2um), standard (~10um), and wide (~25um) spacing between the deflecting fibers. These parameters provided the cell interaction with either several, two, or a single fiber, respectively.

3.1.3 Scaffold Properties

Combining the different diameters and spacing, five varieties of scaffolds were manufactured and used for testing as outlined in Figure 23. These fiber orientations will be

referred to by their diameter (nm) and spacing (um) as (diameter,spacing). All of the fiber nanonets were fused using the previously mentioned desiccator method. By keeping the length of the fiber relatively constant throughout, the main change in environmental stiffness that would be sensed by the cell was due to the changing diameter of the fibers.

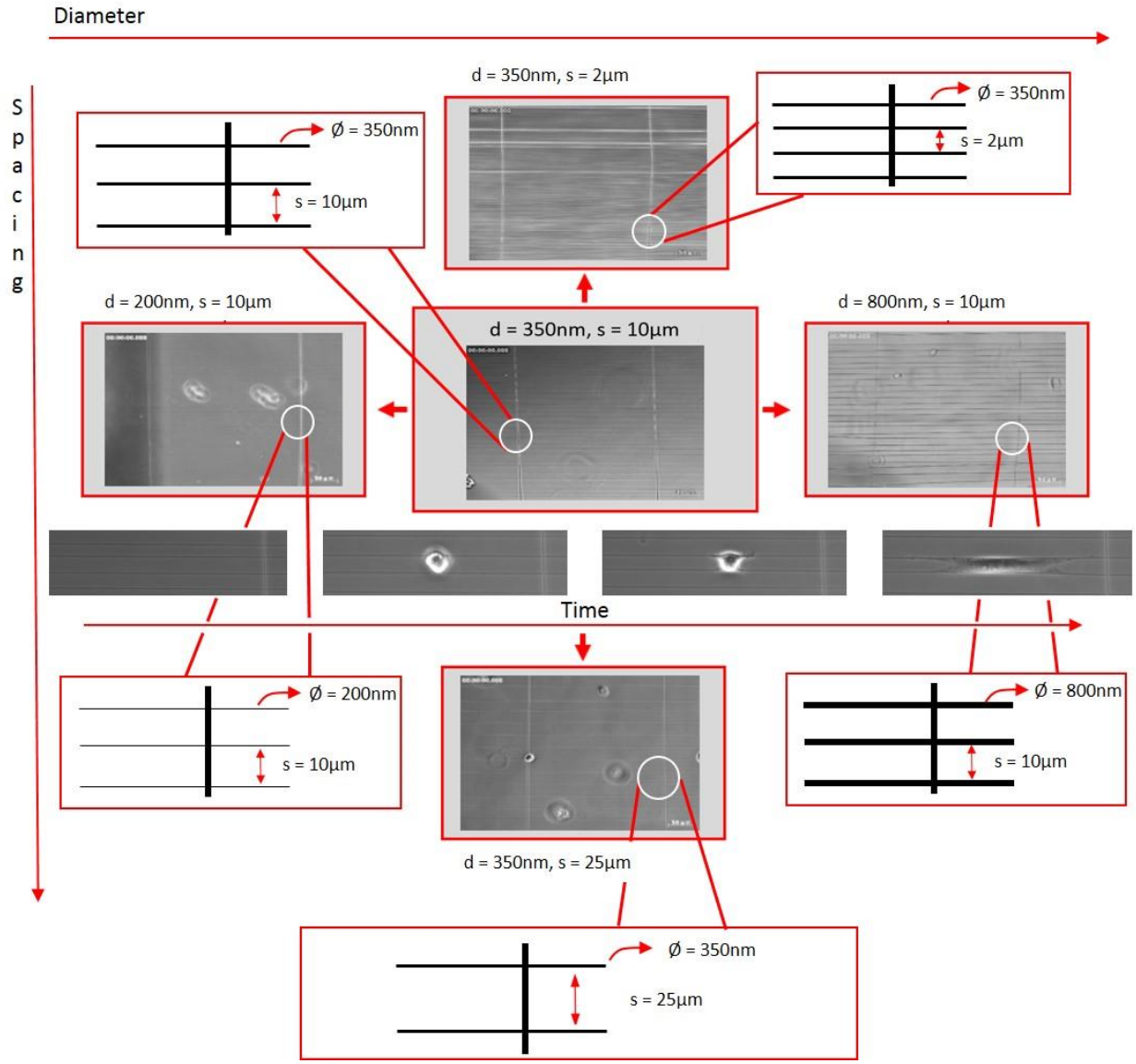

Figure 23. Five different types of scaffolds used in the attachment study.

3.1.4 Platform Setup

One of the main hurdles when attempting cell attachment studies is time frame. Wanting to capture adhesion from the first step requires swift movement from seeding to imaging. Current

seeding protocols for standard experiments have the cell suspension placed on the fibers in the bio-hood and consequently moved to the incubator for attachment. Following this seeding protocol for attachment would be problematic because of the temperature shift during transfer into the microscope. As was mentioned earlier, temperature shifts in the microscope can cause issues at this scale. Whereas earlier this led to drifting of the probe, it can also cause the images to go in and out of focus resulting in unusable videos and a wasted experiment.

To address this, the proven glass-bottom petri dish and CO_2 lid were enlisted to serve as the basis of the cell-attachment platform. Scaffolds were mounted to the petri dishes using vacuum grease, sterilized in 70% ethanol for 10 minutes, rinsed in PBS, and then coated in fibronectin overnight in the incubator at 37°C. On experiment day the dish is moved into the microscope where the CO_2 lid with IO cover are mounted. In earlier drug studies, tubing was placed in the small hole to deliver rapamycin to the cell culture medium. Here, the same approach is used to transfer the cell suspension to the scaffold. The tubing is mounted so that one end is directly over the scaffold. The other end leads outside of the microscope to a luer-lock fitting. This is then left for two hours to reach a steady state temperature within the microscope. Seeding is accomplished by bringing a cell suspension in a syringe and pushing it through the tubing onto the scaffold. Utilizing the definite-focus feature and starting the timelapse before dropping the suspension results in the best results for imaging.

3.1.5 Initial Testing with NIH3T3 Cells

Preliminary attachment experiments were run using NIH3T3 mouse fibroblast cells. The first was run at 10x magnification due to the large suspended area of fibers being 4mm x 4mm. This also resulted in a large number of points in the experiment which led to imaging at every 1.5 minutes as the quickest option possible. Here, a standard scaffold (350nm fibers with 10um

spacing) was used, and the fibers were coated overnight with 2 ug/mL FN, with seeding followed standard protocol. Following the experiment, data was collected on the cell spread area, circularity and force application during attachment. Both spread area and circularity were measured using imageJ software every frame starting at the point the cell would enter the field of view until the area had reached a steady state value. This initial point when each individual cell would enter the field of view would be taken as the zero time point. Using this same starting frame, the deflection of the bottom fiber was also noted with Axiovision software every frame until a relatively constant deflection was achieved.

3.1.5.1 Area Maturation

Cell area was investigated to try and understand the time until steady state spreading was seen. While cell-to-cell heterogeneity will lead to varying total spread area, it is expected to see a relatively consistent time at which that maturation occurs. The original motivation behind this was to note time for mature adhesion formation, with the assumption that at a steady state cell spread area, stable focal adhesions have formed. Figure 24 shows the area change over time of nine 3T3 cells attaching to the fibrous substrate. A regular increasing pattern is seen until around 50 minutes thereafter remaining fairly constant.

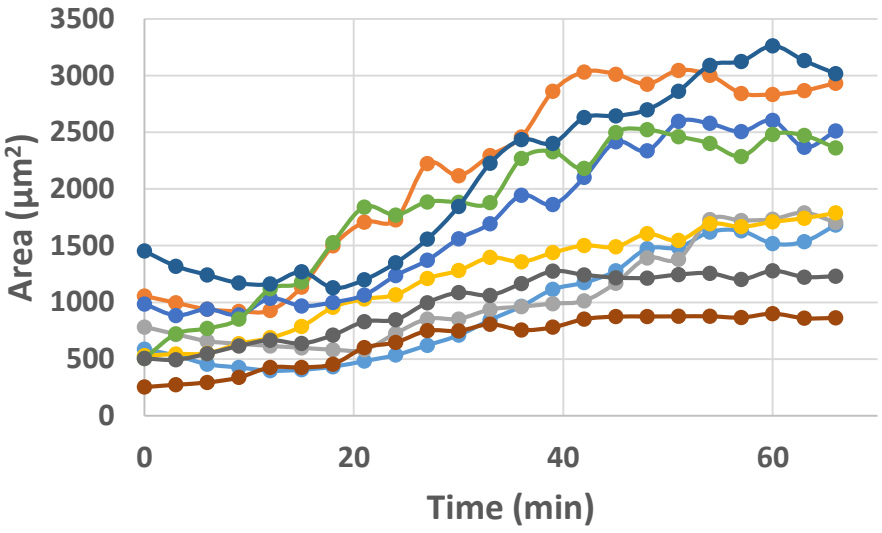

Figure 24. 3T3 cell spread area maturation over time during attachment

3.1.5.2 Circularity Transformation

When cells are in suspension after trypsinization they take on a rounded morphology, which will change as they attach and spread on a substrate. Circularity is calculated as

$$\text{Circ} = \frac{4\pi A}{P^2} \qquad \text{Equation 1}$$

where A is the area and P is perimeter. A value of 1.0 indicates a perfect circle, while approaching 0 is representative of an increasingly elongated shape. Both the actual value of circularity as well as the rate of change can be studied here to investigate the level of isotropic/anisotropic spreading and rate of attachment, respectively. Seen in Figure 25 are the circularity profiles of the same nine cells during attachment. While the initiation time varies from cell-to-cell, the slopes of the profiles are similar. This difference in time to start breaking from a circle is dependent on several factors including location in the suspension and general cell-to-cell heterogeneity, but the similar slopes during the change from a circle to spread and elongated show that spreading is not a random event.

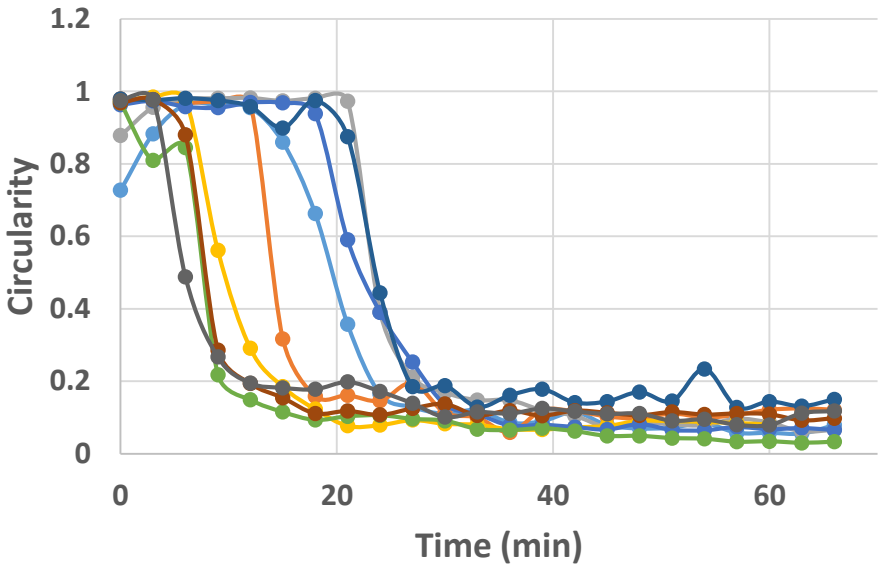

Figure 25. Change in cell circularity over time during attachment

3.1.5.3 Force Signature during Attachment

Utilizing the designed nanonets, fiber deflections were monitored in order to calculate forces associated with cell attachment to the substrate. As mentioned previously, during cell attachment many biological and mechanical events are occurring to sense and adhere to the environment leading to mature focal adhesion formation and contraction is a necessary process for spreading. After a period of time, the force was expected to saturate and hold steady after a certain point signifying stable attachment. Figure 26 shows the attachment force profile for four cells. An interesting feature is the 'negative force' which was defined by a protrusive element during attachment. As seen in Figure 27, on initial sensing of the environment, the cells deflected the fibers outwards with potentially a protrusive force before contracting. After this protrusive force, the cells begin to contract and all seem to saturate around the 45 minute point with mature adhesions formed.

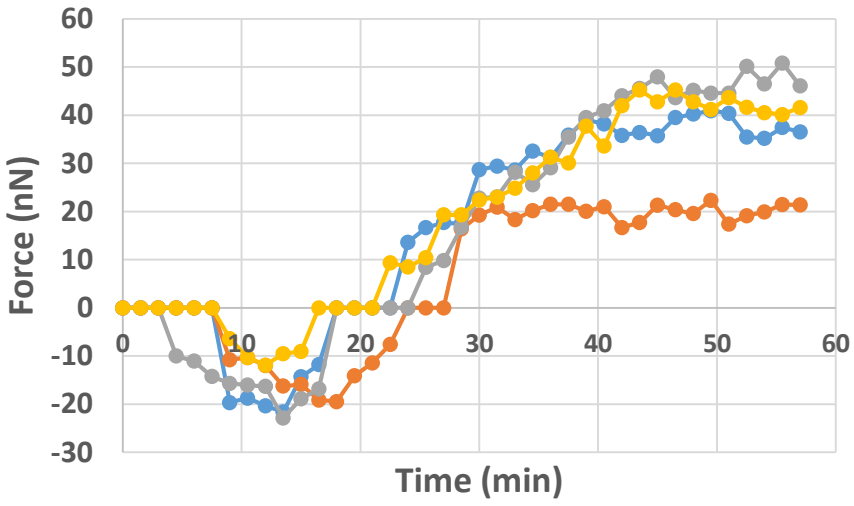

Figure 26. Adhesion force profile during cell attachment.

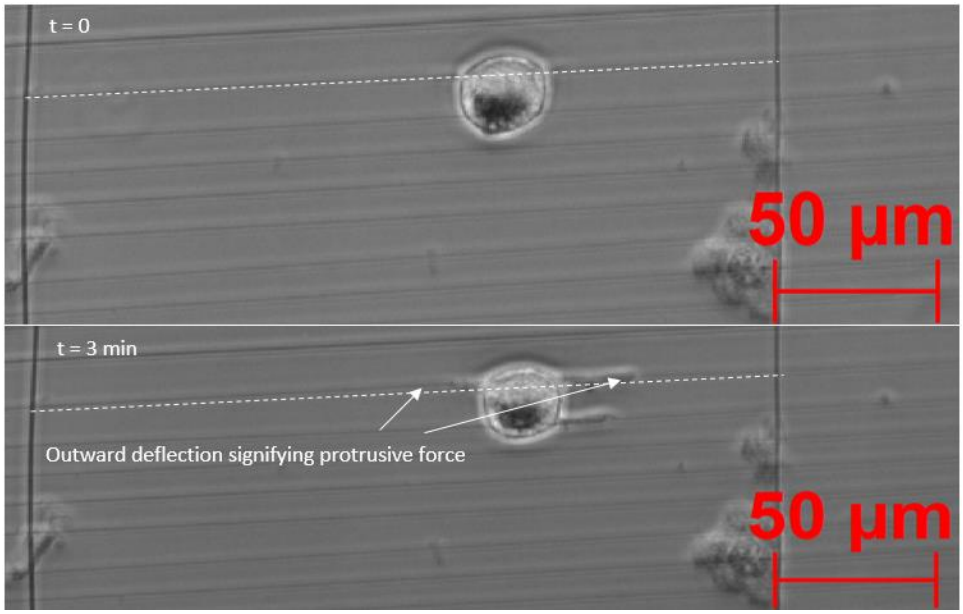

Figure 27. 3T3 cell deflecting fiber outwards on initial attachment to substrate.

3.1.6 Troubleshooting

Following early success with the first 10x experiment, problems arose with cells not attaching. During the experiment, cells would come into view and even interact with the fibers, but they would not commit to attaching and spreading. Scaffold geometries were changed out for the densely (~2um) spaced fibers and even with the cells sitting across multiple fibers they would

not spread. The next step in troubleshooting was trying increasing FN concentrations (4, 8, and 16 ug/mL) to ensure that this biochemical portion was not the cause of cells not attaching, but this did not remedy the situation. To rule out the platform and seeding setup, seeding was attempted using the standard seeding protocol. Again, no attachment was seen. At this point, cell variety was tested by using C2C12 myoblasts, leading to successful attachment on all FN concentrations and confirmation that the older 3T3 cells were the root of the problem. Wanting to study strictly the mechanical influence on attachment and spreading a single FN concentration was chosen to run all experiments with. Initial testing using 8 and 16 ug/mL with C2C12s resulted in cells beginning to spread so quickly that the early stages could potentially be missed. The final concentration chosen was 4ug/mL since it would allow one hour long experiments to capture the entire spreading process while also providing the capability of acquiring early adhesion development. Additionally, while 10x magnification provided a good overview of the attachment process, more detailed information can be extracted with higher magnifications. In order to maximize the probability of choosing a position on the scaffold where a cell will attach, the suspended area was reduced from 16mm^2 to 4mm^2. This allowed for imaging the entire suspended area at a frame rate of one image per minute.

3.2 Spreading Dynamics

3.2.1 Area Maturation

The entire scaffold design space, as described earlier in Figure 23, was used to test the platform in capturing the dynamics of cell attachment and spreading when encountering different microenvironments leading to different cell morphologies. The first area of study, as was done with the 3T3 cell line, was to investigate the area maturation of individual cells attaching to the fibrous substrate. Figure 28 provides an overview of the general area over time trend for all tested

fiber orientations. The fibers with 10um spacing (200/10, 350/10, and 800/10) promote spreading between two suspended fibers, while 2um spacing (350/2) promotes attachment over several (4-7) fibers and 25um spacing (350/25) leads to spindle morphologies on a single fiber as shown in Figure 29.

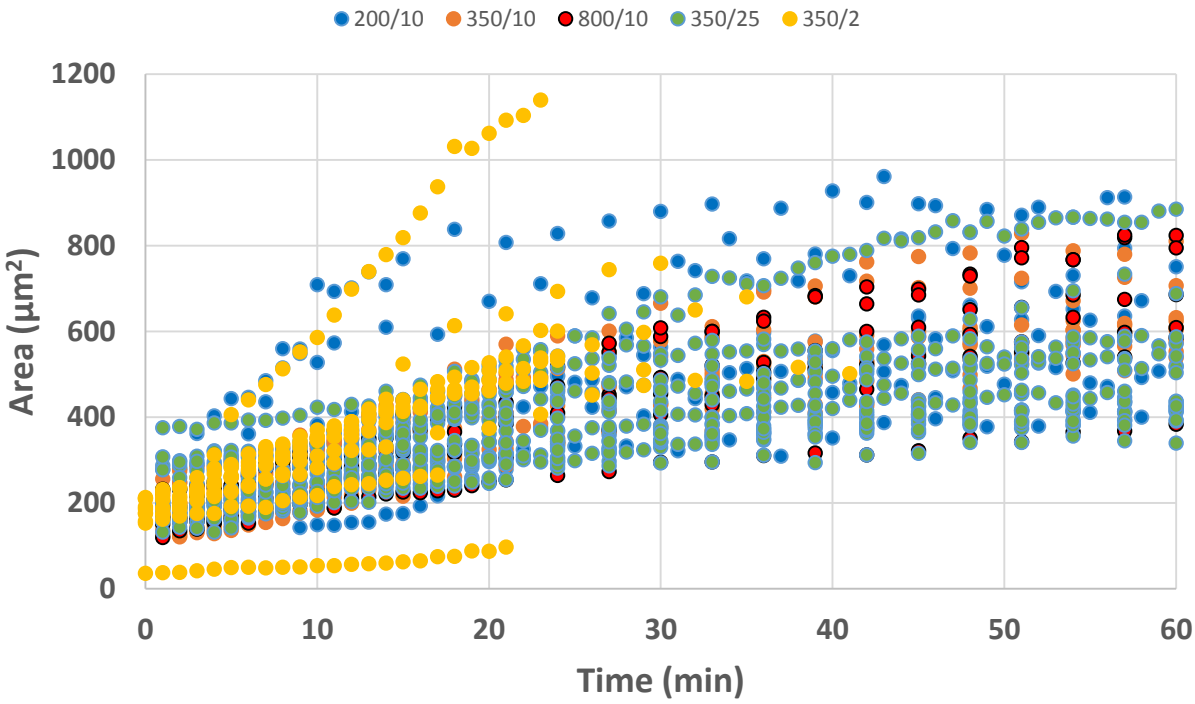

Figure 28. Area versus time comparison over entire design space.

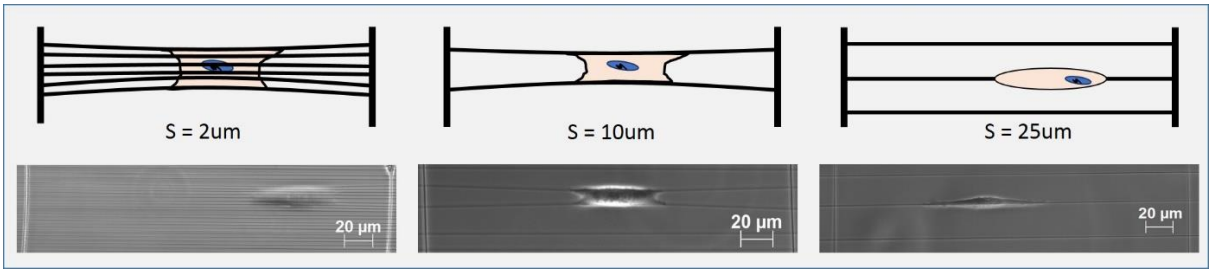

Figure 29. Different cell morphologies achieved with varying spacing of fibers.

Furthermore, because of this difference in morphology is seen, the area maturation was broken down for study by fiber spacing. Figure 30 shows the area development for cells suspended between two fibers on all of the 10um spaced scaffolds of 200nm, 350nm, and 800nm diameter

fibers. Additionally, Figure 31 shows this metric for the 2um spaced fibers, while Figure 32 shows area growth for spindle-shaped cells on 25um spaced fibers.

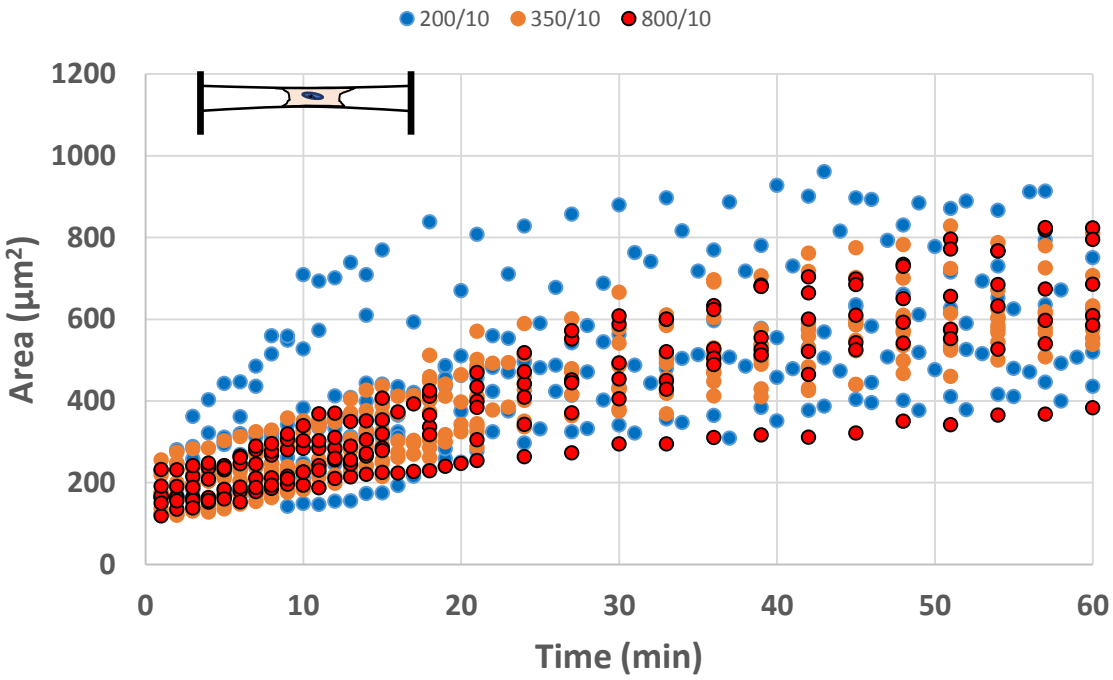

Figure 30. Area versus time comparison on varying diameter fibers, while maintaining 10um spacing.

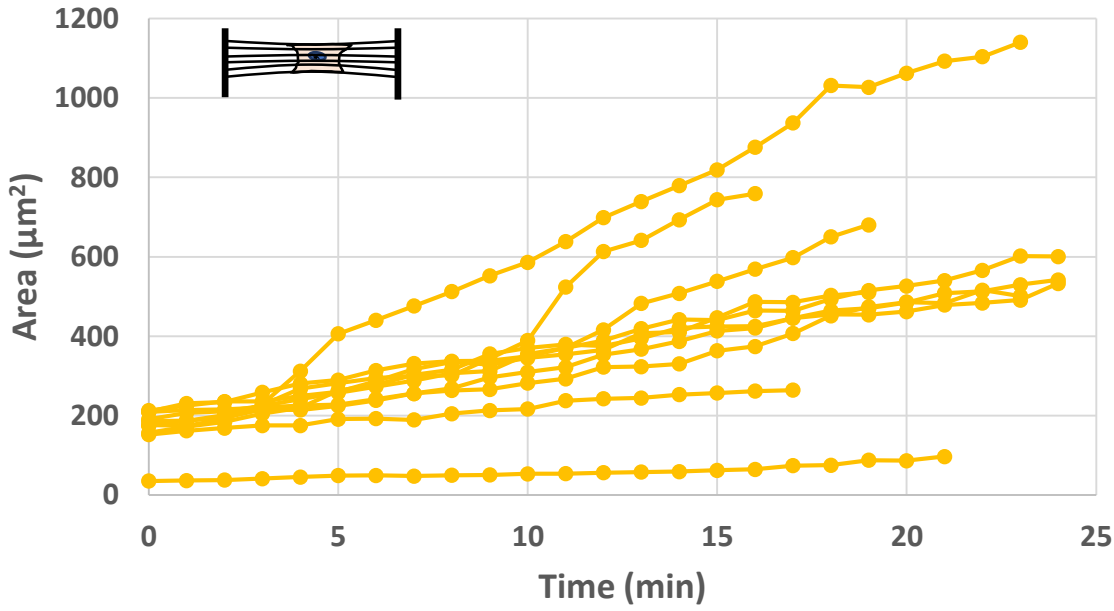

Figure 31. Area versus time maturation of cells suspended across 350nm fibers with 2um spacing.

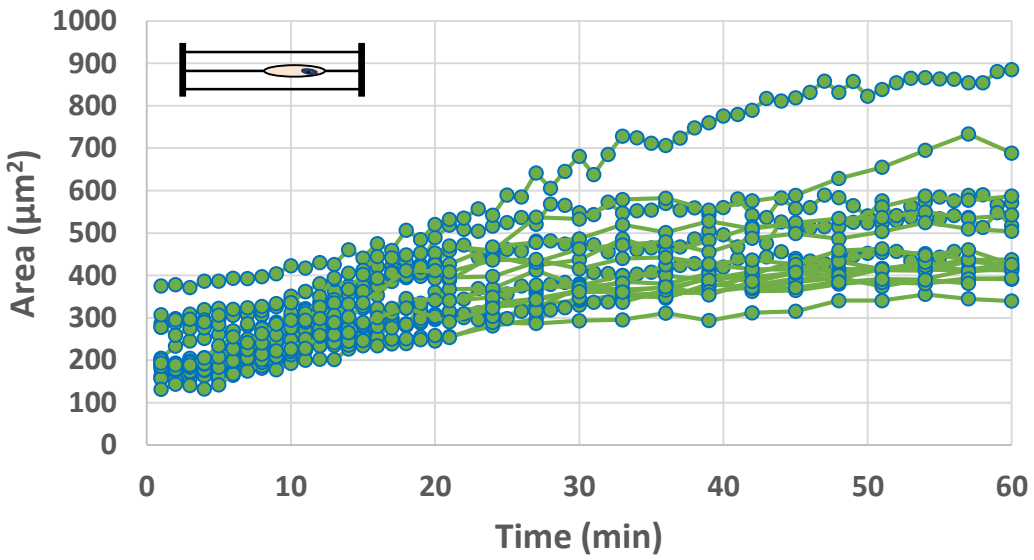

Figure 32. Area versus time maturation of spindle cells on 350nm diameter fibers.

Interestingly, there seems to be a similar pattern to area evolution over time over all different fiber arrangements with an initial linear increase that tapers off to a steady state spread area. There does, however, seem to be a difference in both the rate of growth and overall spread areas. Further population of the data will aid in making distinctions between the geometrical effects of the fiber parameters on area propagation clear.

3.2.2 Circularity Transformation

The change in circularity was studied both temporally and with respect to the spread area. Overall trends for both of these relationships can be seen in Figure 33 and Figure 34, respectively. Regardless of the fiber structure chosen, a similar trend is seen where the circularity of the cells drop quickly in time while simultaneously maintaining a relatively similar spread area. That is, the cells show a break in the circularity very rapidly, while the spread area is not seen to change or grow significantly.

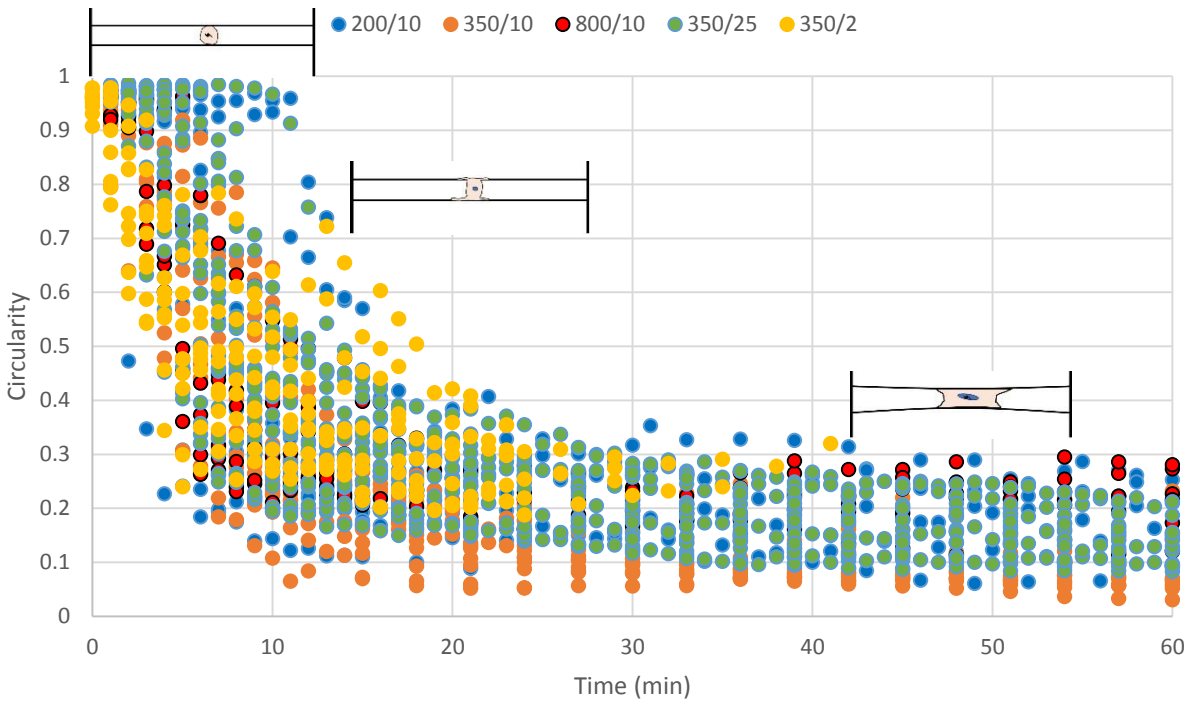

Figure 33. Circularity transformation over time for the entire scaffold design space.

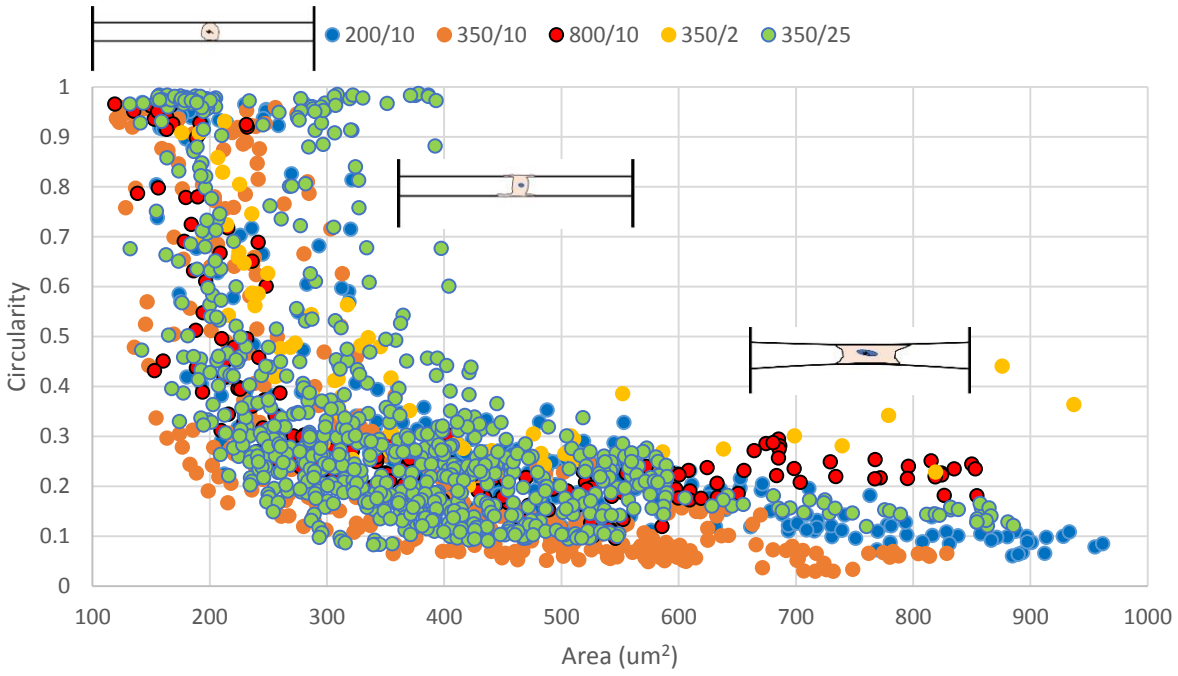

Figure 34. Circularity transformation over area for entire scaffold design space.

Breaking down the data for temporal analysis was done in the same fashion as the area analysis by comparing similar cell morphologies - two fiber, multiple fiber, and spindle. These plots can be seen in Figure 35, Figure 36, and Figure 37, respectively.

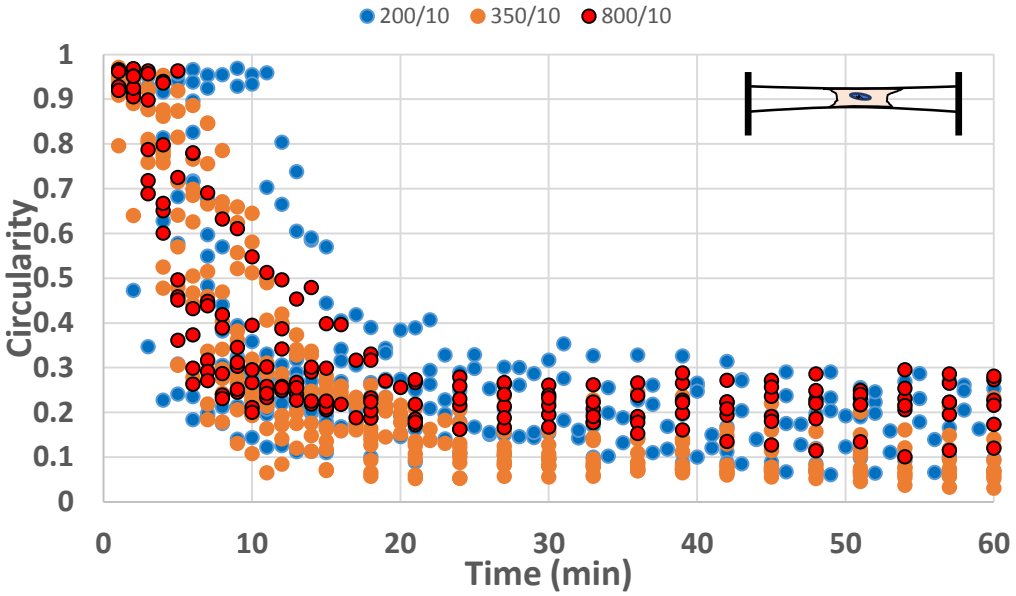

Figure 35. Circularity transformation over time for varying diameter fibers while maintaining 10um spacing.

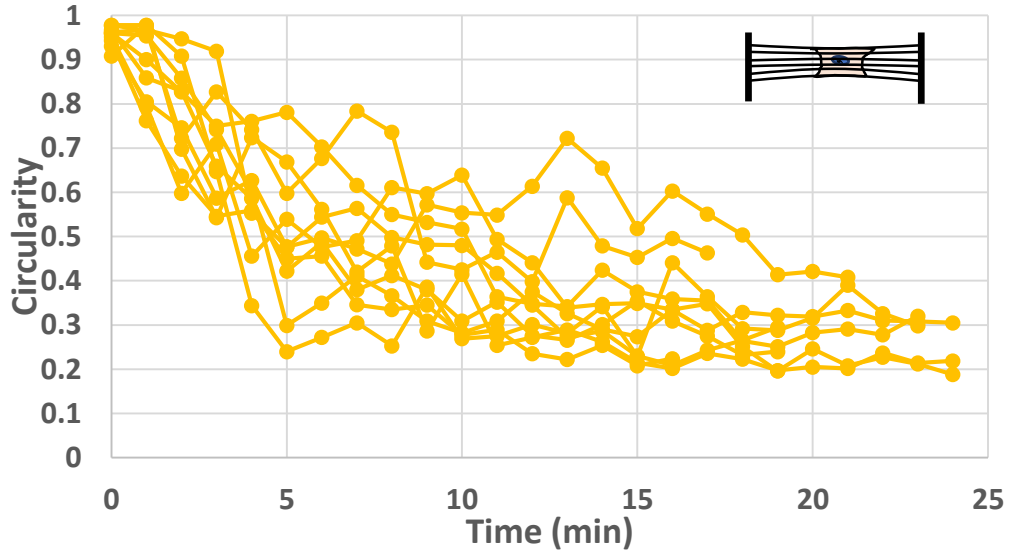

Figure 36. Circularity transformation over time for cells suspended across 350nm fibers with 2um spacing.

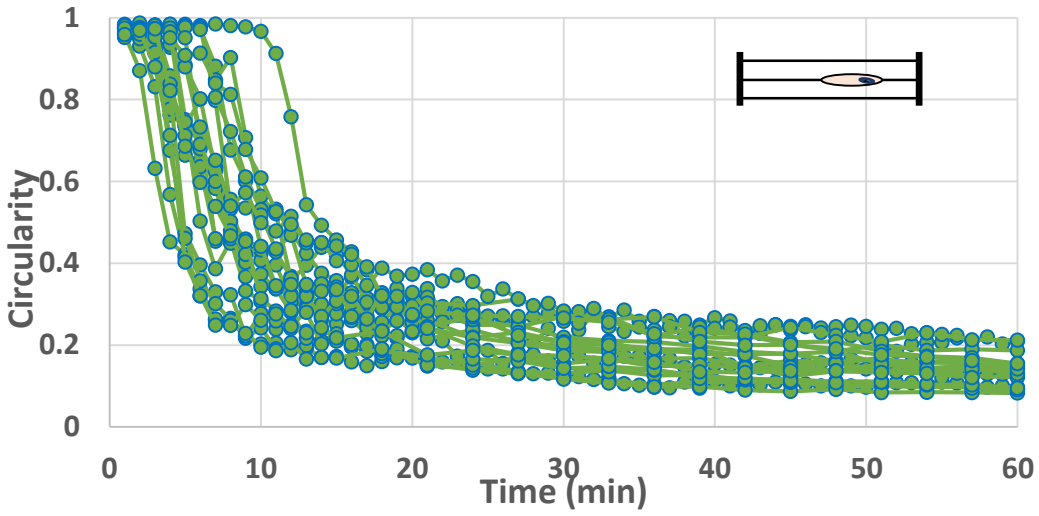

Figure 37. Circularity transformation over time for spindle cells on 350nm diameter fibers.

There was considerably more variation in the resulting circularity after one hour in the two-fiber versus the spindle morphology which also followed a more repeatable evolution. The most outstanding observations is the effect of the more densely spaced fiber deposition every 2um that results in attachment to several fibers. The temporal change here occurs more slowly with a higher circularity maintained for a longer period of time. Although more data needs to be collected and analyzed for concrete effects statements, it appears as if adhesions take longer to develop in cases like this versus having either a single or double fiber attachment geometry.

3.2.3 Force Signature during Attachment

Cell forces during adhesion were monitored for the 350/2, 350/10, and 800/10 scaffolds which allowed for investigating effects of diameter and spacing on force generation independent of each other. Temporal force exertion from the time of initial seeding as well as corresponding cell spread area were studied against the applied cell force. Unlike the 3T3 cell line, there was not a high percentage of cells that were applying protrusive forces on initial attachment before contractile. It is possible that this C2C12 cell line does not apply these protrusive forces during

attachment, or perhaps the imaging restrictions did not capture a minute dislocation of the fibers. As before with circularity, a comparison of all measured scaffolds can be seen in Figure 38 and Figure 39 for force versus time and force versus area, respectively. As expected, the data follows the trend with larger diameter, and therefore higher stiffness, relating to a higher cell contractile force output. Also, a general strengthening is seen over time with forces starting at zero, staying low until a rapid increase, followed by saturation in under one hour.

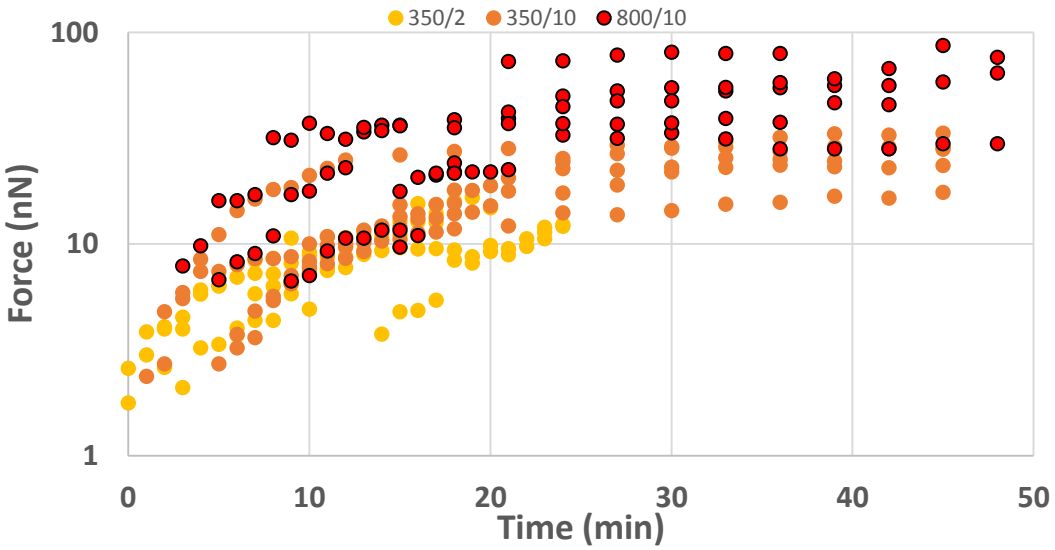

Figure 38. Applied cell force over time for various fiber orientations.

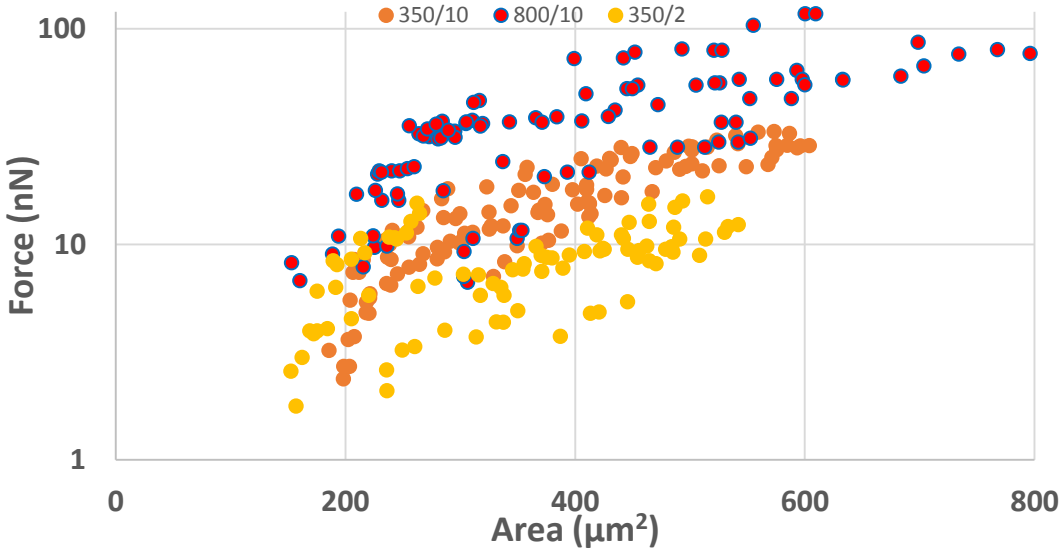

Figure 39. Applied cell force over area for various fiber orientations.

Force versus time trends were individually plotted to examine critical components of the force maturation for each different geometry scaffold. One big component was the inclusion of the 350/2 scaffolds which allowed, for the first time, for the repeatable capture of cell contractile force generation on aligned nanofibers. Although more data needs to be collected, preliminary data shows the feasibility of this study, as well as initial information showing similarities in the force generation scaffolds of varying spacing but different diameter as seen in the 350/2 and 350/10 scaffolds in Figure 41 and Figure 42, respectively. Interestingly on these scaffolds, there was the expected deflection of the outer fibers, but no measureable displacement of the fibers towards the center of the cell. To supplement these observations, cells seeded on these scaffolds were fixed and stained for actin (red), paxillin (green) and the nucleus (blue) as seen in Figure 40. The paxillin, signified by the green, can be seen distributed over all of the fibers meaning that adhesion sites have formed on all of the fibers the cell is sitting on. The lack of deflection on the inside points to the possibility that the cell generates its traction forces towards the cell boundary or that it is simply more difficult to contract the center of the cell body. At the same time, there seems to be a considerable difference when comparing simply diameter variance with constant spacing such as with the 350/10 and 800/10 with much higher forces as seen in Figure 43. Also more apparent when singling out each scaffold type is the no force region on each, followed by a rapid increase in the contractile force application.

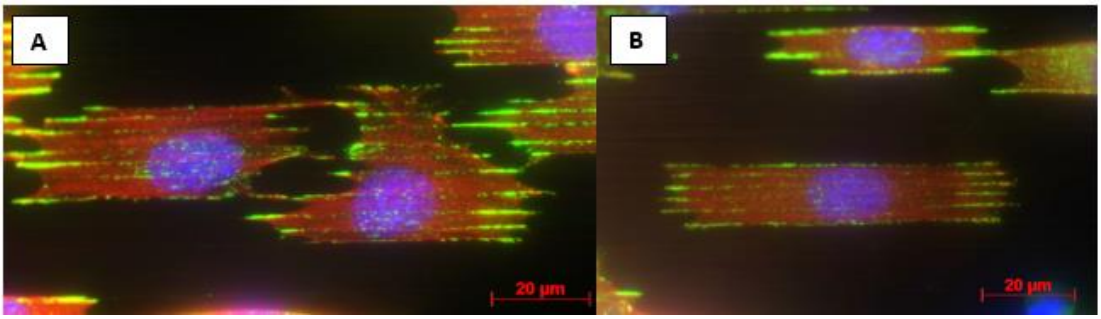

Figure 40. Stained C2C12 cells with red corresponding with actin, green for paxillin, and blue for the nucleus.

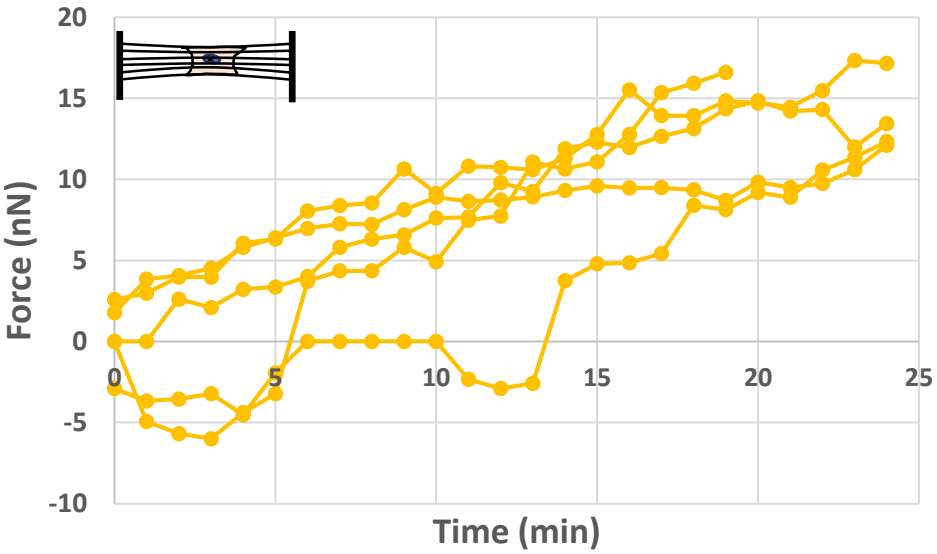

Figure 41. Force output over time on 350nm fibers with 2um spacing

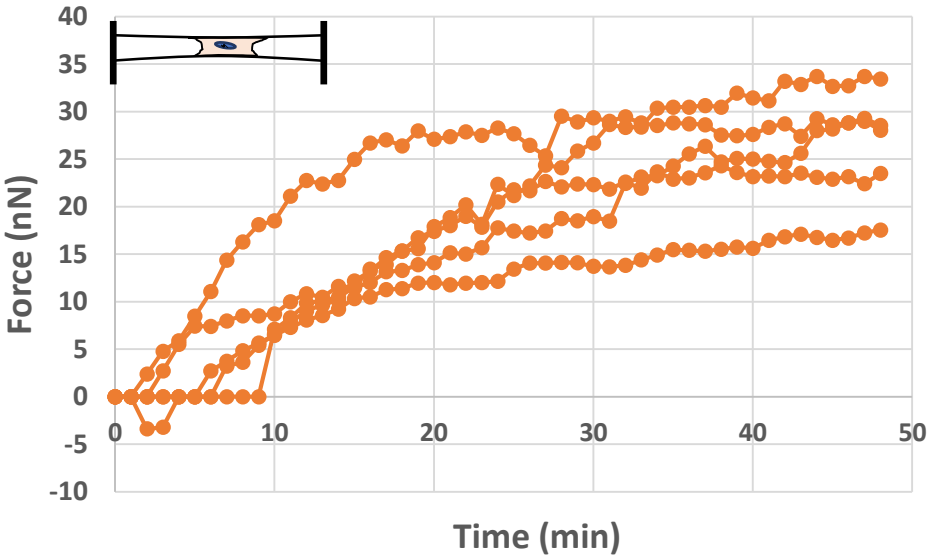

Figure 42. Force output over time on 350nm fibers with 10um spacing

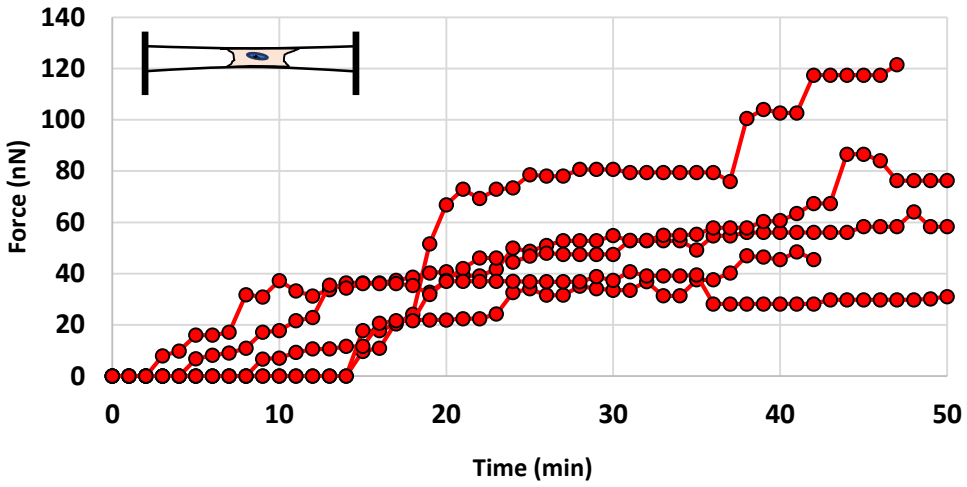

Figure 43. Force output over time on 800nm fibers with 10um spacing

3.2.4 Discussion

It has been stated in literature that cell attachment and spreading occurs over three distinct phases [1,4–8]. Phase 0 involves initial contact and subsequent integrin clustering followed by phase 1 where rapid actin polymerization leads to quick cell spreading and culmination in phase 2 where contractions from the cell are employed to sense the surrounding [38]. A proposed cell attachment map by Wolfenson et al has been reproduced with permission from Elsevier and is included in Figure 44 [38].

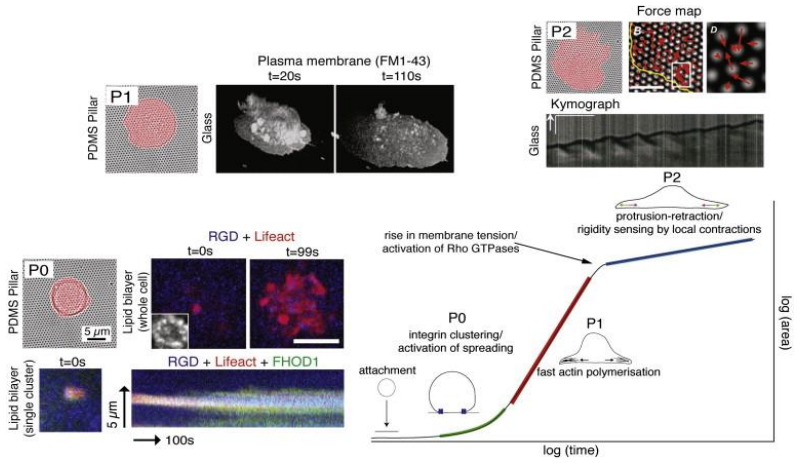

Figure 44. Proposed attachment map by Wolfenson et al. Reprinted from Biophysical Review, 107/11, Haguy Wolfenson, Thomas Iskratsch, and Michael P. Sheetz, Early Events in Cell Spreading as a Model for Quantitative Analysis of Biomechanical Events, 2508-2514, 2014, Used with permission from Elsevier, 2015.

While studies like this provide great insight, the flat and gel microenvironments used are not representative of the native fibrous ECM environment. The platform created here has allowed for the testing of attachment dynamics on fibers for the first time. Looking to characterize an attachment map across fibers, distinct events during the attachment process are dissected and compiled into an attachment map for cells attaching to suspended nanofibers as seen in Figure 45. Similar to P0 shown by Wolfenson et al, a P0 is seen here where there is an initial contact period where the cell commits to adhesion. This phase is characterized by a high circularity of the cell, a maintained area, and either zero or a protrusive force. This changes to P1 as the circularity of the cell breaks and rapidly begins to drop. The following events of P1 involve extensions of protrusions from the cell while the area remains fairly constant relative to the steady state spread area eventually achieved. During P1 the circularity drops to near the final steady state circularity value as well. This is different from the P1 reported by others, which may be due to it being a quick event that is not able to be captured on other assays. Another aspect that is different is that on other flat assays the cell is allowed freedom to spread in any direction and fashion of choice, whereas the a geometrical constraint is applied through these fibers that dictates spreading pattern leading possibly to more anisotropic spreading. However, spreading patterns seen on tightly spaced fibers was visually seen to be more isotropic and this same spreading pattern as on other fibers was seen. Changeover to P2 occurs once the circularity has approached this steady state value. Following this point, there is a concomitant rapid increase in force and spread area until a saturation of both is seen in under an hour. This seems to align with the P1 seen in literature, however, the elements of P2 from literature with environmental sensing through contractions are also a key component.

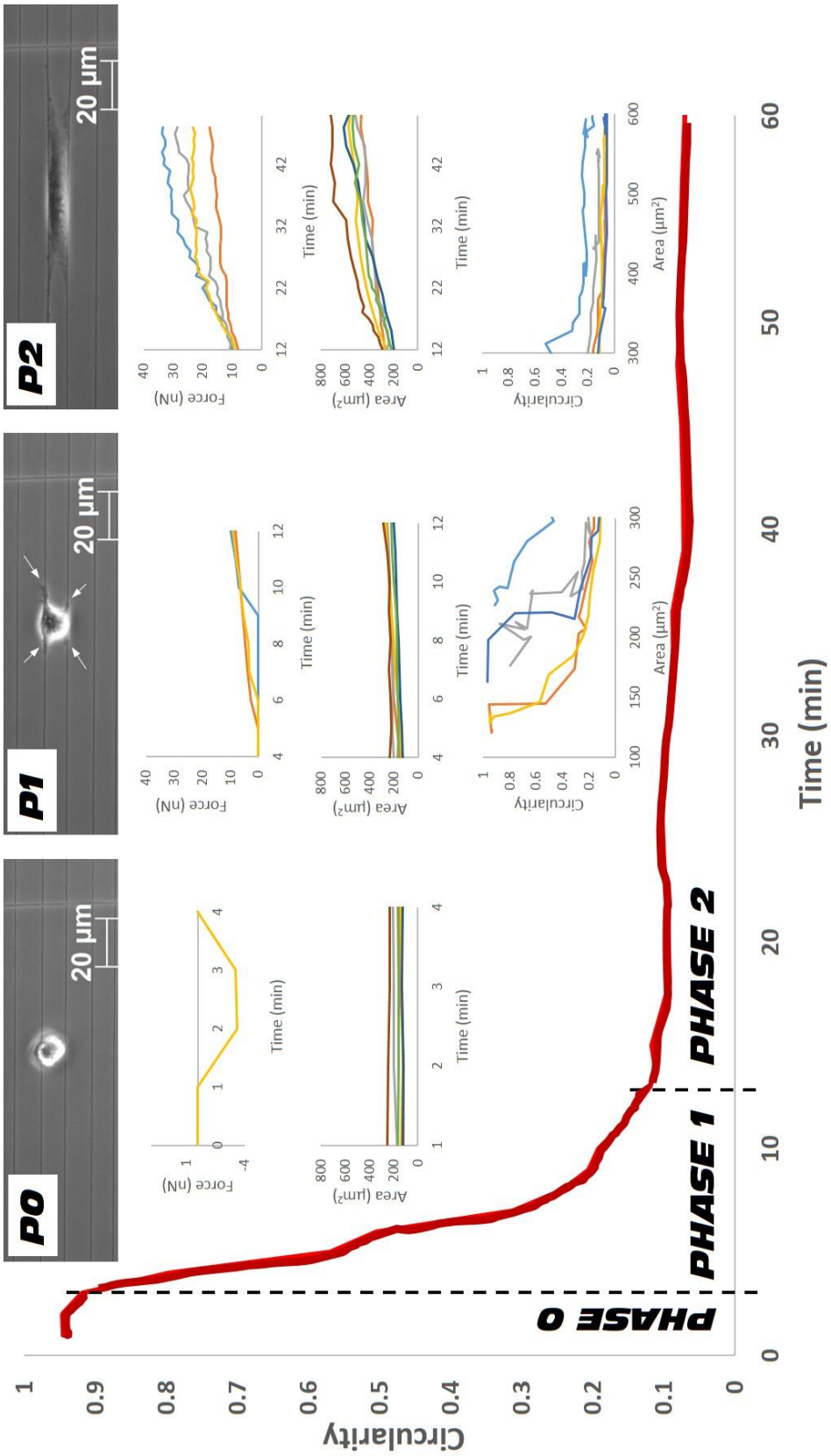

Figure 45. Proposed cell attachment map on fused-fiber nanonets.

3.3 Hook

Cells on substrates are constantly sensing, responding and moving in their environment. On the standard parameter scaffold (d=350m, s=10um) there were instances where the cells would attach to a single fiber and spread following a spindle morphology. Following some of these cells closely revealed an interesting spreading behavior where the cell is putting out filamentous 'hooks' and using these to further attach and apply force. Shown in Figure 46 is one example of the behavior seen. In the first frame, the cell is seen in its regular spindle morphology, followed by the extension of the hook in the second frame. By the third frame a clear deflection in the newly hooked fiber is seen showing force application by the cell on the fiber. While not much is known on the timescales of integrin-ECM contact and bond formation, it has been stated that this junction is incapable of force application [1]. For this reason, we propose that this connection is a purely mechanical process where this hook around the adjacent fiber is made, and through cell-body contraction, force applied.

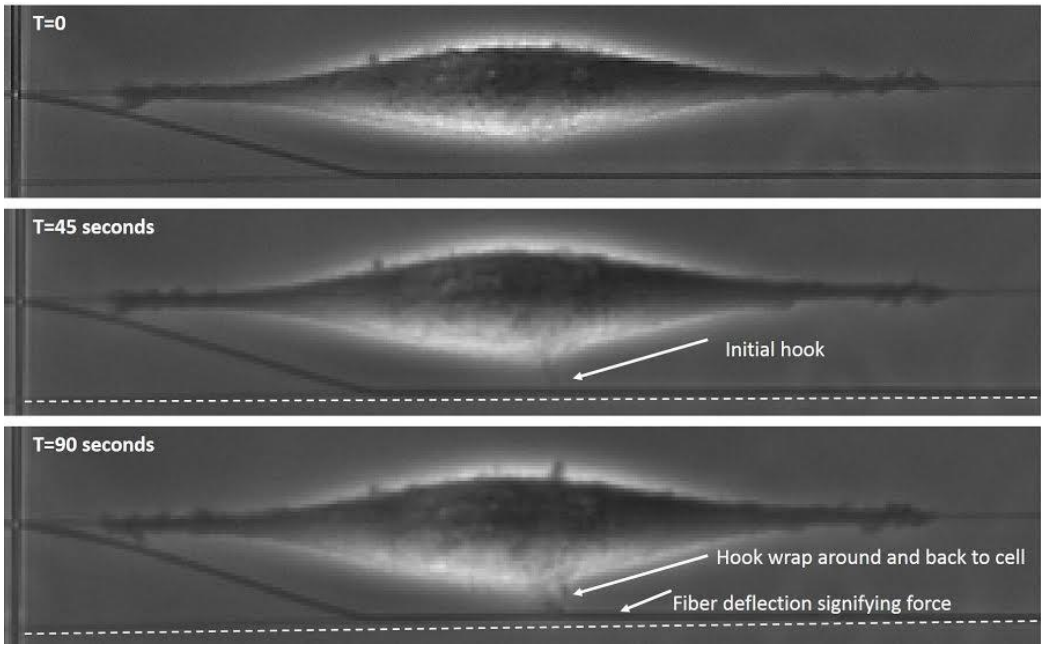

Figure 46. Cell behavior where a spindle cell is seen to send out filamentous hooks and apply force to an adjacent fiber.

Chapter 4: Contributions

Cell attachment studies are still a relatively new focus in the field. Previous work has begun to show some of the events in early cell adhesion and spreading, namely the three phases of spreading. It has also been shown that cell body contraction is necessary for spreading. The other main property studied is spread area maturation, which has been shown by some groups to follow a sigmoidal shape. This study has been able to capture spread area maturation, change in circularity, and detailed force application by cells during the attachment process.

This study is the foundation of knowledge using fibers for understanding this initial cell-ECM adhesion and spreading. Platform development has been performed to get to this point with preliminary attachment data collected using C2C12 mouse myoblasts. The system has been setup for more detailed investigations comparing different cell lines and disease states for future work. The STEP fibers utilized in the system have the capability of showing protrusive forces in attachment for the first time.

Beyond simply attachment experiments, this designed system will continue to be useful for detailed studies of drug testing and other work that requires high quality images, probe work, or use of petri dishes instead of the standard 6-well plates currently in place. As projects like this are completed, doors open as to what can be accomplished within the STEP Lab. Internally, each study and project done bring forth more knowledge and remove limitations allowing for unparalleled growth.

Chapter 5: Future Directions

5.1 Dual Probe Holder

As mentioned previously, outside-in force experiments were initially conducted with a single probe, but moved towards two probes with one on either side of the cell so as not to induce a bias. The method of setting up the dual probes on the original design, seen in Figure 47A was difficult and required a lot of manual tweaking. This original design was then modified as seen in Figure 47B to provide slots for the micropipettes to sit, but the angles on the slots did not allow for enough clearance for the condenser of the microscope.

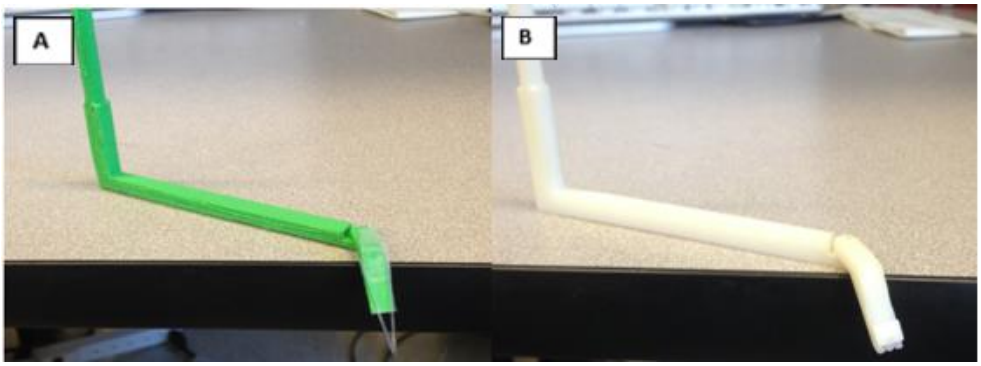

Figure 47. (A) Original dual probe holder requiring manual positioning of pipettes. (B) Revised design with slots for pipettes.

To address these issues, modifications were made to give a wider base on which to attach the pipettes. This would allow easier positioning, as well as giving a greater angle so that the pipette tips could be positioned closer to each other. This angle of 77.4 degrees was calculated so that based on a 63 mm pipette that could be consistently pulled, the tips would line up 150 um apart from each other. On this design, there was a lip at the back from which to align the probes so that the tips would be at the same distance and the grooves were utilized for consistent positioning. Version one of this update is seen in Figure 48.

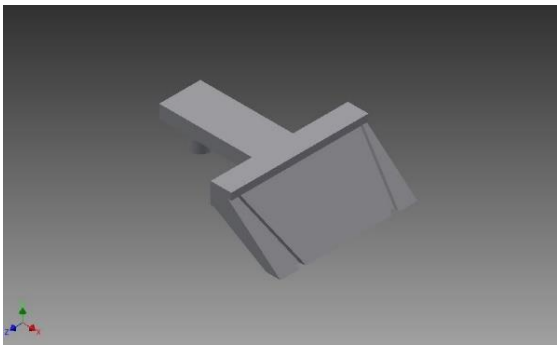

Figure 48. Version one of the updated dual probe holder utilizing a wider base and a rear lip to line up pipette tips.

The design was then taken a step further as seen in Figure 49 to allow variable spacing between the probes. This would be useful for when a cell has a wider adhesion on the fibers since the pipettes could now be widened to accommodate this.

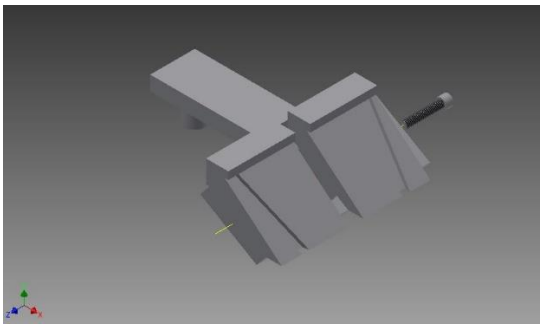

Figure 49. Update to version one of the dual probe holder which now allows for variable pipette spacing.

A 3d printed version of the standard spacing and a mock-up of the variable spacing were made to check for clearance in the microscope and demonstrate a proof-of-concept for the designs, both of which can be seen in Figure 50. The fixed-spacing model was manufactured using extrusion-based additive manufacturing, while the variable-spacing model utilized styrene to represent the plates on a commercially-available micropositioner.

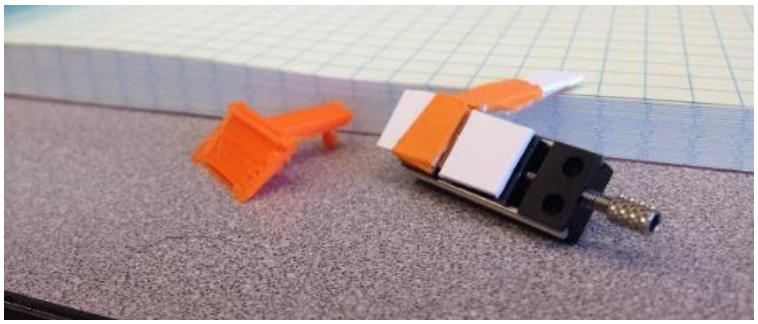

Figure 50. Early proof-of-concept prototypes of the fixed-spacing and variable-spacing dual probe holder

Through further discussion with manufacturing at Virginia Western Community College, it was decided to use the existing micropositioner and attach the plates for holding the pipettes. The CAD model was updated for this revision as shown in Figure 51A and the final product was then CNC-machined out of aluminum as shown in Figure 51B and Figure 51C.

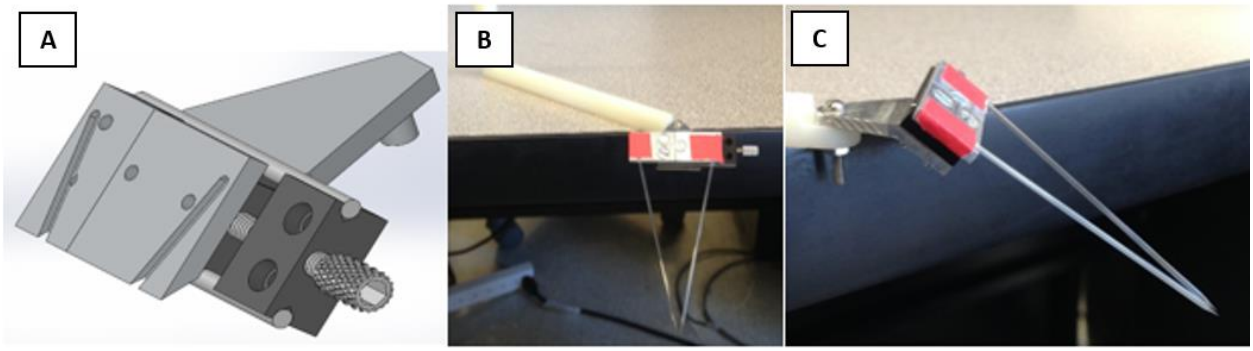

Figure 51. (A) Updated CAD model incorporating existing micropositioner. (B) Front view of new dual probe holder with glass micropipettes installed. (C) Side view of new dual probe holder.

After taking delivery, the new dual probe holder was tested for accuracy. This was done by mounting the glass micropipettes and then measuring final position of the tips. Figure 52 shows the closest position, giving approximately 33um between the tips of the probes. The error in final position of the tips of the pipettes was also noted, with the one on the left approximately 193 um further forward than the one on the right. By watching the change in z-position on the motorized stage display, the error in the z-height was found to be approximately 150um. Unfortunately, these errors will not allow for this current setup to work since the fiber networks have much closer spacing between adjacent fibers. This error come from the manufacturing process where the CNC

mill used does not allow for the precision required at the micro and nano scale these experiments are run at.

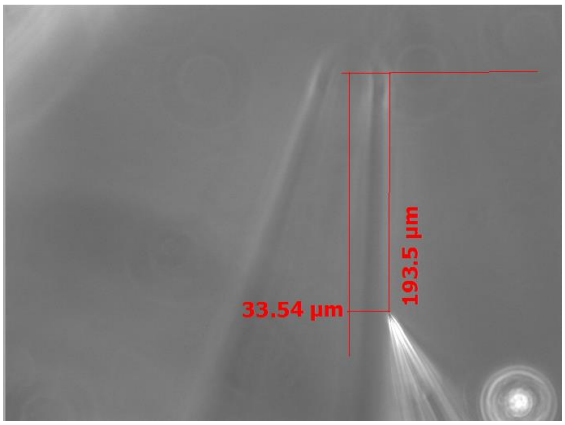

Figure 52. Image taken in the scope to determine the accuracy of the manufactured dual probe holder.

5.2 Single-Cell Aspiration

Isolating specific cells from a substrate can be very useful when trying to study cell-to-cell heterogeneity. Properties such specific morphologies, attachment on different diameter fibers, or even leader cells can be studied. Leader cells are defined as those that are the first to break away from a large mass of cells. In an experimental setup cells are seeded on the edge of the scaffold where they form a monolayer. Once confluent they begin to move out onto the fibers as seen in Figure 53.

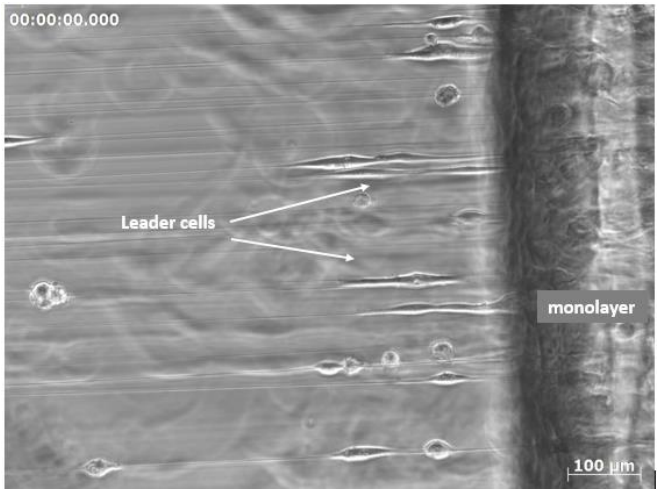

Figure 53. Experimental setup of leader cell formation on STEP fibers.

One method that can be used to try and capture these cells from STEP fibers is micropipette aspiration, where negative pressure applied from a syringe will pull its surroundings, including a cell, inside. This aspiration method can take direct advantage of the system designed in this work when using the CO_2 lid for probe work. Preliminary work has shown the capability of aspiration in capturing cells from STEP fibers. Glass micropipettes were manufactured using a Sutter P-1000 micropipette puller with the tips cut back further manually using a razor blade so that the inner diameter was approximately 50um. In Figure 54A one of these glass micropipettes is shown near a cell suspended on a single nanofiber, and followed in Figure 54B is after the aspiration where the cell is no longer visible.

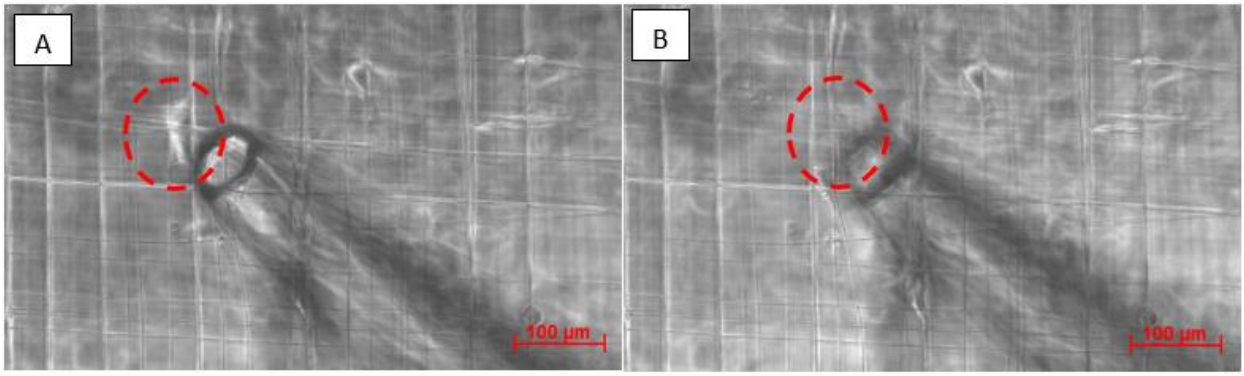

Figure 54. Example of aspiration with the micropipette. (A) The circled DBTRG cell is attached to the substrate. (B) The cell has been aspirated into the micropipette.

Although this method has been shown to work in isolating cells, preliminary experiments showed unofficial results of approximately 30% viability of aspirated cells. Part of this low percentage of viability was thought to be due to the surface finish on the micropipette which was very rough and jagged and was potentially puncturing the cells. Methods including using a Sutter VS-10 beveler and fire-polishing the pipette tip using the P-1000 puller were investigated to try and enhance surface finish. Through decreasing grit size of the beveler pad, surface finish was made much smoother, as shown in scanning electron microscope (SEM) images of the probes seen

in Figure 55B vs Figure 55A. Including a fire-polish step leads to an even finer surface finish as seen in Figure 55C.

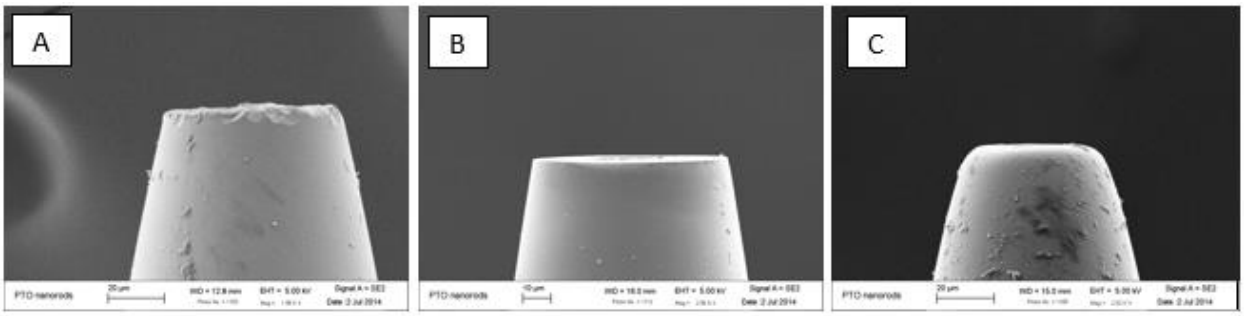

Figure 55. (A) Initial pipette with coarse grinding from bevler. (B) Adding fine grit grinding from beveler. (C) Adding fire-polishing after grinding to tip of micropipette.

After determining optimal conditions for aspiration to maximize viability, the next step would be to design a setup where the cell can be lysed as quickly as possible. Lysing breaks apart the cell and allows for the capture of the genetic information which can permit studies on internal biological differences in cells of interest. The process of lysing releases the contents of the cell into the immediate surrounding fluid, so media uptake is to be minimized. One idea tested was applying a filter to the end of a micropipette that would allow for the capture of the cell on the end of the filter while allowing media to flow through. This probe would then be moved to a lysing solution where the cell contents would be harnessed. Attempts to perform this manually have been unsuccessful simply due to the scale at which this needs to be completed. Figure 56A shows a polyvinylidene fluoride (PVDF) filter with 0.1um pores applied to the end of a glass micropipette. The extra overhang beyond the tip was cut as close as manually possible, and then tested for aspiration. Displayed in Figure 56B is the pipette placed in the microscope where it was seen that there was still a considerable portion of the filter extending past the tip and distorting imaging as well as disturbing the fiber nanonet.

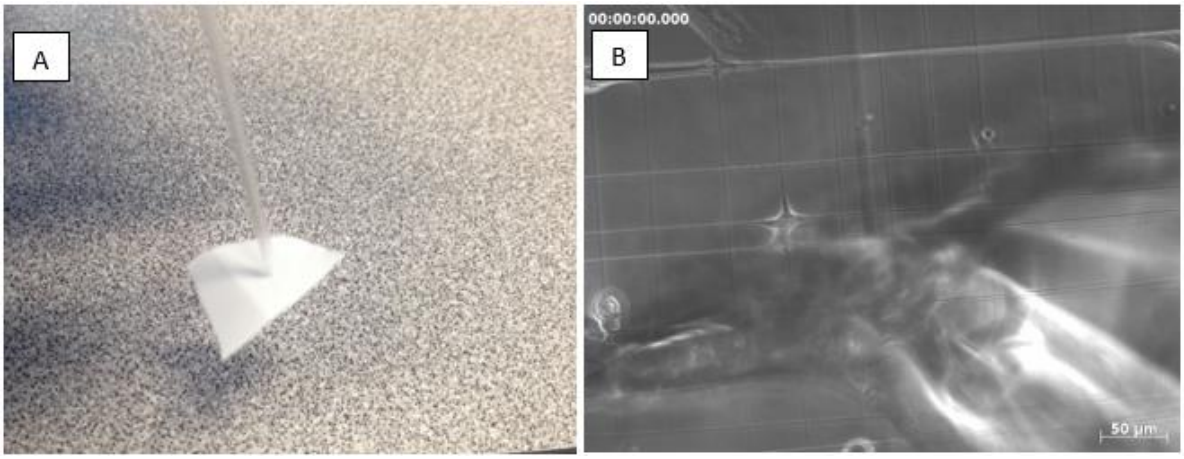

Figure 56. (A) PVDF filter applied to the end of the glass micropipette (B) The filter on the end of the pipette disrupts imaging and contacts the fiber nanonets.

The next idea for improvement was to try and insert the filter just inside the tip of the pipette. This was attempted by using a pipette with a smaller diameter tip to push the filter inside one with a larger (~50um) inner diameter. One of the main difficulties was lining the two probes up since the smaller probe was aiming for a 50um position. When they were able to line up, other problems arose from the pipette puncturing of the filter which would make it unusable in this application. To try and address this issue, PS beads ~25um in diameter were to be placed on the tip of the pipette. This proved very difficult to line up manually with inconsistent results. Many of the troubles arose from performing tasks at this scale manually. Moving forward, it would be useful to look into automated filter application or even possibly the use of hydrogels as the porous substance to trap the cell at the tip. Seen in Figure 57 is a design idea for lining up the probes based on a laser positioning system. This would provide reliable location mapping so that the probes would align with each other perfectly and make application simpler.

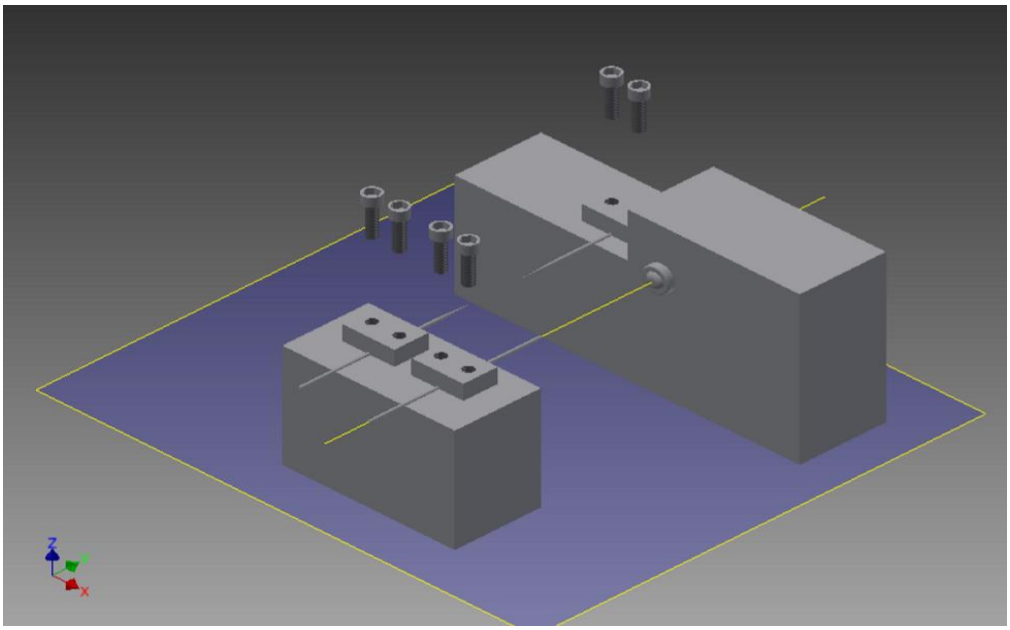

Figure 57. Proposed automated filter application system. The yellow line represents a laser that will set a reference location so that the pipettes shown to the left line up perfectly with each other.

5.3 Localized Drug Delivery

One of the main uses of the probe system is in drug studies. One area for potential improvement and investigation moving forward would be in the delivery of the drug. In the work on the MEF cells, rapamycin was added into the culture medium so that the entire dish concentration was at a desired amount. Possible uncertainty exists with this approach because it must be assumed that all cells in the entire dish are receiving the same concentration of drug at the same time and this may not necessarily be true. Additionally, this is a very inefficient method of performing drug studies because it creates a situation where an entire scaffold is subjected to a drug while only a single cell can be tested at a time. This results in very slow data collection and an excess waste of scaffolds. Looking into locally delivering the drug would be helpful in making more efficient use of time and resources moving forward with these studies. One proposed solution for this would be to use a glass micropipette with a cured hydrogel such as polyethylene glycol diacrylate (PEG-DA) at the tip. This micropipette can be controlled using a motorized

micropositioner similarly to how OI probe work is done. The drug can then diffuse from the hydrogel to the cell of interest. Knowing the diffusive properties will allow one to calculate how far and quickly the drug will diffuse, which will allow testing on other cells within the scaffold known to not have been effected by the drug yet. A study on this local drug delivery, like aspiration work, can also take advantage of the system designed here.

5.4 OI Forces of Cells Spread on Numerous Fibers

In this study we not only show attachment and spreading over multiple fibers, we show for the first time cell contractile force generation over more than two aligned and suspended nanofibers. This was a great preliminary look at increasing the cell contact area on a controlled fibrous environment, where it was noted at a majority of the deflections in the fibers were seen on the extreme top and bottom. However, OI forces have innately been able to show much more information in the past such as ultimate adhesion strength and this would be great to look at focal adhesion distribution when there are fibers in the middle of the cell body as well as towards the outside.

5.5 Further Attachment investigations

Moving forward with attachment investigations there are a plethora of directions to explore. One in particular that many other groups have studied is the effect of varying the concentration of FN on attachment. In uncharacterized preliminary work here, it was noted that changing the concentration did have an effect on the initial attachment time, but it would also be useful to study the effect on force generation, total spread area, and time to spread, especially since there have been contradicting statements in literature and this platform is able to, uniquely from the others done, provide a native ECM-like fibrous environment. Along with varying the concentration of FN, different ligands such as collagen could also be compared on their effect on

attachment and spreading. After effect of ligand and ligand concentration are looked into, different cell lines can be studied to compare adhesion dynamics between cell lines and even between healthy and diseased states. Another area of work that would be immensely useful for not only this, but many other studies in the STEP Lab as well would be a form of automated analysis. Right now all circularity, area, and deflection data needs to be collected post-experiment manually which is very time consuming and subject to possible user-to-user bias. Implementing an automated analysis system would speed up analysis time and allow more focus to be put on running experiments.

References

[1] Shawn P. Carey, J. M. C. and C. A. R.-K., 2011, "Forces During Cell Adhesion and Spreading: Implications for Cellular Homeostasis," Stud Mechanobiol Tissue Eng Biomat, **4**(September 2010), pp. 29–69.

[2] Dubin-Thaler, B. J., Giannone, G., Döbereiner, H.-G., and Sheetz, M. P., 2004, "Nanometer analysis of cell spreading on matrix-coated surfaces reveals two distinct cell states and STEPs.," Biophys. J., **86**(March), pp. 1794–1806.

[3] Döbereiner, H.-G., Dubin-Thaler, B., Giannone, G., Xenias, H. S., and Sheetz, M. P., 2004, "Dynamic phase transitions in cell spreading.," Phys. Rev. Lett., **93**(10), p. 108105.

[4] Fouchard, J., Bimbard, C., Bufi, N., Durand-Smet, P., Proag, a, Richert, a, Cardoso, O., and Asnacios, a, 2014, "3D cell-body shape dictates the onset of traction force generation and growth of focal adhesions," Proc. Natl. Acad. Sci. U. S. A., **111**(36).

[5] Dubin-Thaler, B. J., Hofman, J. M., Cai, Y., Xenias, H., Spielman, I., Shneidman, A. V., David, L. a., Döbereiner, H. G., Wiggins, C. H., and Sheetz, M. P., 2008, "Quantification of cell edge velocities and traction forces reveals distinct motility modules during cell spreading," PLoS One, **3**(11).

[6] Étienne, J., and Duperray, A., 2011, "Initial dynamics of cell spreading are governed by dissipation in the actin cortex," Biophys. J., **101**(3), pp. 611–621.

[7] Lam Hui, K., Wang, C., Grooman, B., Wayt, J., and Upadhyaya, A., 2012, "Membrane dynamics correlate with formation of signaling clusters during cell spreading," Biophys. J., **102**(7), pp. 1524–1533.

[8] Pietuch, A., and Janshoff, A., 2013, "Mechanics of spreading cells probed by atomic force microscopy.," Open Biol., **3**(7), p. 130084.

[9] Bereiter-Hahn, J., Lück, M., Miebach, T., Stelzer, H. K., and Vöth, M., 1990, "Spreading of trypsinized cells: cytoskeletal dynamics and energy requirements.," J. Cell Sci., **96 (Pt 1)**, pp. 171–188.

[10] Cuvelier, D., Théry, M., Chu, Y.-S., Dufour, S., Thiéry, J.-P., Bornens, M., Nassoy, P., and Mahadevan, L., 2007, "The universal dynamics of cell spreading.," Curr. Biol., **17**, pp. 694–699.

[11] Reinhart-King, C. a, Dembo, M., and Hammer, D. a, 2005, "The dynamics and mechanics of endothelial cell spreading.," Biophys. J., **89**(1), pp. 676–689.

[12] Nisenholz, N., Rajendran, K., Dang, Q., Chen, H., Kemkemer, R., Krishnan, R., and Zemel, A., 2014, "Active mechanics and dynamics of cell spreading on elastic substrates," Soft Matter, **10**, pp. 7234–7246.

[13] Giannone, G., Dubin-Thaler, B. J., Döbereiner, H. G., Kieffer, N., Bresnick, A. R., and Sheetz, M. P., 2004, "Periodic lamellipodial contractions correlate with rearward actin waves," Cell, **116**(3), pp. 431–443.

[14] Cavalcanti-Adam, E. A., Volberg, T., Micoulet, A., Kessler, H., Geiger, B., and Spatz, J. P., 2007, "Cell spreading and focal adhesion dynamics are regulated by spacing of integrin ligands.," Biophys. J., **92**(8), pp. 2964–2974.

[15] Cramer, L. P., and Mitchison, T. J., 1995, "Myosin is involved in postmitotic cell spreading," J. Cell Biol., **131**(1), pp. 179–189.

[16] Goffin, J. M., Pittet, P., Csucs, G., Lussi, J. W., Meister, J. J., and Hinz, B., 2006, "Focal adhesion size controls tension-dependent recruitment of α-smooth muscle actin to stress fibers," J. Cell Biol., **172**(2), pp. 259–268.

[17] Schwarz, U. S., and Gardel, M. L., 2012, "United we stand - integrating the actin cytoskeleton and cell-matrix adhesions in cellular mechanotransduction," J. Cell Sci., **125**(13), pp. 3051–3060.

[18] Ponti, a, Machacek, M., Gupton, S. L., Waterman-Storer, C. M., and Danuser, G., 2004, "Two distinct actin networks drive the protrusion of migrating cells.," Science, **305**(5691), pp. 1782–1786.

[19] Bardsley, W. G., and Aplin, J. D., 1983, "Kinetic Analysis of Cell Spreading," **373**, pp. 365–373.

[20] Nain, A. S., Sitti, M., Jacobson, A., Kowalewski, T., and Amon, C., 2009, "Dry Spinning Based Spinneret Based Tunable Engineered Parameters (STEP) Technique for Controlled and Aligned Deposition of Polymeric Nanofibers.," Macromol. Rapid Commun., **30**(16), pp. 1406–12.

[21] Nain, A. S., Phillippi, J. a, Sitti, M., Mackrell, J., Campbell, P. G., and Amon, C., 2008, "Control of cell behavior by aligned micro/nanofibrous biomaterial scaffolds fabricated by spinneret-based tunable engineered parameters (STEP) technique.," Small, **4**(8), pp. 1153–9.

[22] Reinhart-King, C. a., 2008, "Endothelial Cell Adhesion and Migration," Methods Enzymol., **443**(08), pp. 45–64.

[23] Evans, E. a, and Calderwood, D. a, 2007, "Forces and bond dynamics in cell adhesion.," Science, **316**(5828), pp. 1148–53.

[24] Benoit, M., Gabriel, D., Gerisch, G., and Gaub, H., 2000, "Discrete interactions in cell adhesion measured by single-molecule force spectroscopy," Nat. Cell Biol., **2**(June), pp. 313–317.

[25] Friedrichs, J., Legate, K. R., Schubert, R., Bharadwaj, M., Werner, C., Müller, D. J., and Benoit, M., 2013, "A practical guide to quantify cell adhesion using single-cell force spectroscopy," Methods, **60**, pp. 169–178.

[26] Canale, C., Petrelli, A., Salerno, M., Diaspro, A., and Dante, S., 2013, "A new quantitative experimental approach to investigate single cell adhesion on multifunctional substrates.," Biosens. Bioelectron., **48C**, pp. 172–179.

[27] Xie, H., Yin, M., Rong, W., and Sun, L., 2014, "In Situ Quantification of Living Cell Adhesion Forces: Single Cell Force Spectroscopy with a Nanotweezer," Langmuir.

[28] Kuo, C.-W., Shiu, J.-Y., Chien, F.-C., Tsai, S.-M., Chueh, D.-Y., and Chen, P., 2010, "Polymeric nanopillar arrays for cell traction force measurements.," Electrophoresis, **31**(18), pp. 3152–3158.

[29] Harris, A. K., Wild, P., and Stopak, D., 1980, "Silicone rubber substrata: a new wrinkle in the study of cell locomotion.," Science, **208**, pp. 177–179.

[30] Dembo, M., and Wang, Y., 1999, "Stresses at the cell-to-substrate interface during locomotion of fibroblasts," Biophys. J., **76**(January), pp. 2307–2316.

[31] Wang, J., and Nain, A. S., 2014, "Suspended Micro/Nano fi ber Hierarchical Biological Sca ff olds Fabricated Using Non-Electrospinning STEP Technique," Langmuir, (30), pp. 13641–13649.

[32] Meehan, S., and Nain, A. S., 2014, "Role of Suspended Fiber Structural Stiffness and Curvature on Single-Cell Migration, Nucleus Shape, and Focal-Adhesion-Cluster Length," Biophysj, **107**(11), pp. 2604–2611.

[33] Sharma, P., Sheets, K., Subbiah, E., and Nain, A. S., 2013, "The Mechanistic Influence of Aligned Nanofiber Networks on Cell Shape, Migration and Blebbing Dynamics of Glioma Cells," Integr. Biol., (In Press).

[34] Sharma, P., Kim, A., Gill, A., Wang, J., Sheets, K., Behkam, B., and Nain, A. S., 2014, "Aligned and suspended fiber force probes for drug testing at single cell resolution.," Biofabrication, **6**(4), p. 045006.

[35] Parsons, S. J., and Parsons, J. T., 2004, "Src family kinases, key regulators of signal transduction.," Oncogene, **23**, pp. 7906–7909.

[36] Chu, P.-H., Tsygankov, D., Berginski, M. E., Dagliyan, O., Gomez, S. M., Elston, T. C., Karginov, A. V, and Hahn, K. M., 2014, "Engineered kinase activation reveals unique morphodynamic phenotypes and associated trafficking for Src family isoforms.," Proc. Natl. Acad. Sci. U. S. A., **111**(34), pp. 12420–5.

[37] Thomas, S. M., and Brugge, J. S., 1997, "Cellular functions regulated by Src family kinases.," Annu. Rev. Cell Dev. Biol., **13**, pp. 513–609.

[38] Wolfenson, H., Iskratsch, T., and Sheetz, M. P., 2014, "Biophysical Review Early Events in Cell Spreading as a Model for Quantitative Analysis of Biomechanical Events," Biophysj, **107**(11), pp. 2508–2514.

Appendix A: Uniform Distributed Load Force Model Derivation

The following derivation for force was provided by Ji Wang assuming UDL on the nanofibers. This derivation accounts for the tension that is built into the fiber structure when spinning.

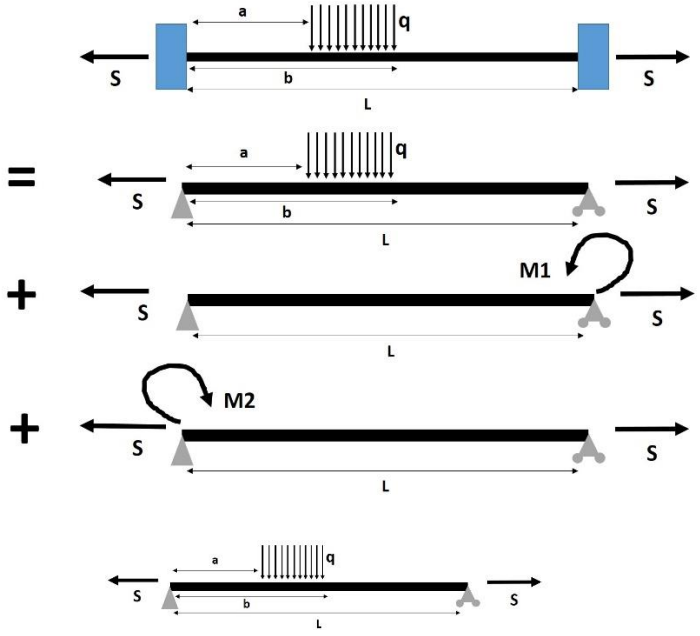

Deflection curve of the portion left to the distributed load:

$$y = -\int_a^b \frac{q\sinh(\lambda c)dc}{S\lambda\sinh(\lambda L)}\sinh(\lambda x) + x\int_a^b \frac{qcdc}{SL}$$

$$= \frac{-q\sinh(\lambda x)}{S\lambda^2\sinh(\lambda L)}[\cosh(\lambda b) - \cosh(\lambda a)] + \frac{xq}{2SL}(b^2 - a^2)$$

$$(0 < x < a)$$

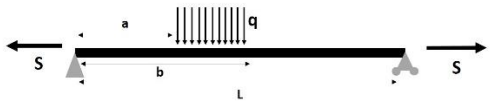

Deflection curve of the portion right to the distributed load:

$$y = -\int_a^b \frac{q\sinh(\lambda(L-c))dc}{S\lambda\sinh(\lambda L)}\sinh(\lambda(L-x)) + (L-x)\int_a^b \frac{q(L-c)dc}{SL}$$

$$= \frac{q\sinh(\lambda(L-x))}{S\lambda^2\sinh(\lambda L)}[\cosh(\lambda(L-b)) - \cosh(\lambda(L-a))] - \frac{q(L-x)}{2SL}[(L-b)^2 - (L-a)^2]$$

$$(b < x < L)$$

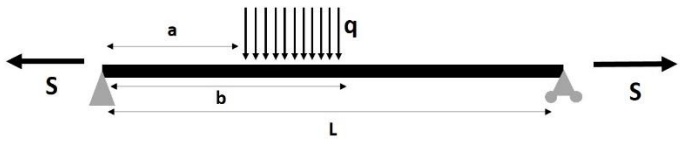

Deflection curve of the loaded portion :

$$y = -\int_a^{L-x} \frac{qdc\sinh(\lambda c)\sinh(\lambda x)}{\lambda S\sinh(\lambda L)} + x\int_a^{L-x} \frac{qcdc}{SL} - \int_{L-x}^b \frac{qdc\sinh(\lambda(L-c))\sinh(\lambda(L-x))}{S\lambda\sinh(\lambda L)} + \int_{L-x}^b \frac{qdc(L-c)(L-x)}{SL}$$

$$= -\frac{q\sinh(\lambda x)}{S\lambda^2\sinh(\lambda L)}[\cosh(\lambda(L-x)) - \cosh(\lambda a)] + \frac{qx}{2SL}[(L-x)^2 - a^2]$$

$$+ \frac{q\sinh(\lambda(L-x))}{S\lambda^2\sinh(\lambda L)}[\cosh(\lambda(L-b)) - \cosh(\lambda x)] - \frac{q(L-x)}{2SL}[(L-b)^2 - x^2]$$

$$(a < x < b)$$

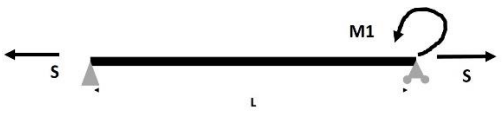

$$M_1=\int_a^b \frac{qdc(c\lambda-1)}{\lambda(\lambda L-2)}=\frac{q(b-a)[\frac{1}{2}(a+b)\lambda-1]}{\lambda(\lambda L-2)}$$

$$y=\frac{q(b-a)[\frac{1}{2}(a+b)\lambda-1]}{\lambda(\lambda L-2)S}(\frac{x}{L}-\frac{\sinh(\lambda x)}{\sinh(\lambda L)})$$

$$M_2=\int_a^b \frac{qdc(\lambda L-c\lambda-1)}{\lambda(\lambda L-2)}=\frac{q(b-a)[\lambda L-1-\frac{1}{2}\lambda(b+a)]}{\lambda(\lambda L-2)}$$

$$y=\frac{q(b-a)[\lambda L-\frac{1}{2}(a+b)\lambda-1]}{\lambda(\lambda L-2)S}(\frac{L-x}{L}-\frac{\sinh(\lambda x)}{\sinh(\lambda L)})$$

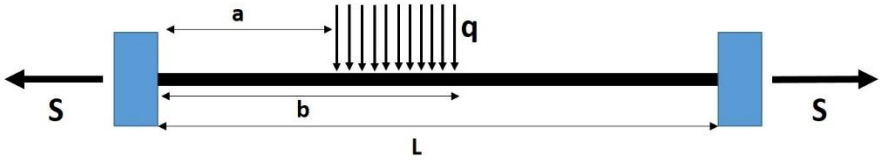

Equation:

$$y=-\frac{q\sinh(\lambda x)}{S\lambda^2\sinh(\lambda L)}[\cosh(\lambda(L-x))-\cosh(\lambda a)]+\frac{qx}{2SL}[(L-x)^2-a^2]$$
$$+\frac{q\sinh(\lambda(L-x))}{S\lambda^2\sinh(\lambda L)}[\cosh(\lambda(L-b))-\cosh(\lambda x)]-\frac{q(L-x)}{2SL}[(L-b)^2-x^2]$$
$$-\frac{q(b-a)[\frac{1}{2}(a+b)\lambda-1]}{\lambda(\lambda L-2)S}(\frac{x}{L}-\frac{\sinh(\lambda x)}{\sinh(\lambda L)})-\frac{q(b-a)[\lambda L-\frac{1}{2}(a+b)\lambda-1]}{\lambda(\lambda L-2)S}(\frac{L-x}{L}-\frac{\sinh(\lambda x)}{\sinh(\lambda L)})$$

$$(a<x<b)$$

Appendix B: MEF Seeding and Experiment Protocol

Seeding process:

1. Wash cells 2x with PBS
2. Add 500uL Trypsin for 5 minutes
3. Add appropriate amount of 10% FBS media to flask and seed ~50uL onto scaffold
4. Allow cells to attach to fiber ~2 hours
5. Fill petri dish with 10% FBS media
6. 30 minutes before running experiment switch media to 5% FBS media (4mL)

Experiment Process:

1. After scope has gotten up to temperature ~30minutes, begin probe pulls (1x every 3 mintutes)
2. After 30 minutes, add rapamycin (solution is made with rapamycin mixed with 1mL 2% FBS media so that final concentration of rapamycin in 5mL of petri dish is 500nM)